Theoretical study of mixing in liquid clouds. Part 1: classical concepts

(revised version, 21 May 2016)

Alexei Korolev[1], Alex Khain[2], Mark Pinsky[2], and Jeffrey French[3]

[1] Environment Canada, Cloud Physics and Severe Weather Section, Toronto, Canada

[2] Department of Atmospheric Sciences, the Hebrew University of Jerusalem, Israel

[3] University of Wyoming, Laramie, WY, USA

Correspondence to: A. Korolev (alexei.korolev@canada.ca)

Abstract

The present study considers final stages of in-cloud mixing in the framework of classical concept of homogeneous and extreme inhomogeneous mixing. Simple analytical relationships between basic microphysical parameters were obtained for homogeneous and extreme inhomogeneous mixing based on the adiabatic consideration. It was demonstrated that during homogeneous mixing the functional relationships between the moments of the droplets size distribution hold only during primary stage of mixing. Subsequent random mixing between already mixed parcels and undiluted cloud parcels breaks these relationships. However, during extreme inhomogeneous mixing the functional relationships between the microphysical parameters hold both for primary and subsequent mixing. The obtained relationships can be used to identify the type of mixing from in situ observations. The effectiveness of the developed method was demonstrated using in-situ data collected in convective clouds. It was found that for the specific set of in-situ measurements the interaction between cloudy and entrained environments was dominated by extreme inhomogeneous mixing.

1 Introduction

Turbulent mixing is an important non-adiabatic process in the atmosphere that to a large extent determines spatial gradients of many thermodynamic (e.g. temperature, humidity) and cloud microphysical parameters (e.g. hydrometeor concentrations, extinction coefficient, condensed water content) and as such, needs to be properly described in numerical simulations of clouds and weather predictions. Entrainment and mixing occurs during the entire lifetime of a cloud and is active not only near cloud edges, but it is important throughout the whole cloud volume. Mixing of cloudy and entrained air results in changes to the shape of the droplet size distribution through partial droplet evaporation and can also lead to changes in droplet concentration through complete evaporation of some fraction of droplets and dilution. The shape of the droplet size distribution plays key role in the initiation of precipitation and radiative properties of clouds.

The treatment of mixing in numerical simulations of clouds and precipitation formation remains a challenging problem. Besides the issues related to the way to describe mixing in numerical schemes, there is a fundamental problem of identifying a scenario or path, that mixing events should follow. Through the pioneering works of Latham and Reed (1977) and Baker et al. (1980) two explicitly alternative scenarios of mixing were identified. In the first scenario turbulent mixing rapidly stirs the environment homogenizing the fields of temperature and humidity. Following that, all of the droplets undergo partial evaporation under the same conditions. The result of this mixing is a droplet population with reduced sizes, but a total number of droplets remains unchanged. This type of mixing is referred to as *homogeneous*. In the second scenario mixing occurs more slowly such, that the population of droplets experiences different amount of sub-saturation. Some number of droplets completely evaporates, while others experience no evaporation until the entirety of the entrained air becomes saturated. Following that, turbulence mixes the rest of the droplets with the saturated, but droplet-free environment. During this type of mixing the size of droplets remains unchanged; however, their total number is reduced. This type of mixing is called *extreme inhomogeneous*. The intermediate case when some fraction of droplets evaporates partially, another other fraction evaporates completely, and a third fraction remains unchanged is in some works referred to as inhomogeneous (e.g. Baker and Latham, 1980).

The conditions for homogeneous and extreme inhomogeneous mixing and their effects on precipitation formation have been debated in cloud physics over forty years. There are a number of numerical simulations and theoretical efforts on studying different aspects of mixing and its effect

on cloud microphysics (e.g. Baker and Latham, 1979, 1982; Jensen and Baker, 1989; Su et al., 1998; Lasher-Trapp et al., 2005; Jeffrey, 2007; Andrejczuk et al., 2009; Kumar et al., 2013; Jarecka et al., 2013; Lu et al. 2011, 2014; Tolle and Krueger 2014; and many others). A comprehensive review of the works on the effect of turbulence and mixing on cloud droplet formation can be found in Devenish et al. (2012).

A number of studies were dedicated to identifying type of mixing based on in-situ observations. Most of the previous observations provided evidence supporting inhomogeneous mixing (e.g. Hill and Choularton, 1985; Paluch, 1986; Bower and Choularton,1988; Blyth and Latham, 1991; Gerber et al., 2008, Lu et al. 2011; Beals et al. 2015). However, works of Jensen and Baker (1989), Paluch and Baumgardner (1989), Burnet and Brenguier (2007), Lehmann et al. (2009), Lu et al. (2011) suggested occurrence of homogeneous mixing. So, at the moment it appears that both types of mixing may occur in liquid clouds. However, the environmental conditions governing one or the other type of mixing remain not well understood.

Early experimental work on identifying type of mixing from in-situ observations were based on the analysis of spatial variability of the shapes of individual droplet size distributions (e.g. Paluch and Knight, 1984; Paluch, 1986; Bower and Choularton, 1988). The effectiveness of this method involving the analysis of a large number of individual size spectra turned out to be quite low. Another technique utilized expected functional relationships between droplet concentration (N) and droplet diameter (D) specific to each type of mixing. Thus, during extreme inhomogeneous mixing the droplet size is expected to remain unchanged, whereas the concentration will vary. During homogeneous mixing the droplet size and concentration in cloud will be related to each other in a certain way, depending on the mixing fraction and the humidity of the entrained air. This fact was used in observational studies for identifying the type of mixing from "mixing diagrams" that related N and D_v for different regimes of mixing (e.g. Burnet and Brenguier, 2007; Gerber et al., 2008; Lehmann et al., 2009).

The use of mixing diagrams to some extent facilitated identification of type of mixing. However, in many cases scatter in the relationships between N vs. D_v was too large, hindering identification of the type of mixing (Burnet and Brenguier, 2007). To resolve this problem many researchers used other complementary measurements supporting identification of the type of mixing (e.g. Gerber et al., 2008; Lehmann et al., 2009).

Besides the effect on N and D_v, the type of mixing is anticipated to manifest itself in relationships between other moments of the droplet size distribution, $f(D)$. Such relationships may provide insight into the mixing process and identify type of mixing. With the exception of the work by Hill and Choularton (1985), who correlated concentration and liquid water content, there have been few attempts to use any other microphysical parameters for identification of type of mixing.

In order to fill this gap, this study presents a theoretical analysis of relationships between different moments of $f(D)$ within the framework of homogeneous and extreme inhomogeneous mixing. The analysis is focused on the first four moments of $f(D)$ corresponding to the droplet concentration N (0^{th} moment), integral diameter $N\overline{D}$ (1^{st} moment), extinction coefficient β (2^{nd} moment), liquid water mixing ratio q (3^{rd} moment) and mean volume diameter D_v (mixed 3^{rd} and 0^{th} moment). It is shown that the newly obtained relationships between the moments provide a more robust identification of type of mixing from in-situ measurements as compared to conventional $N - D_v^3$ relationships used in mixing diagrams. Relationships between moments may be useful for parameterization of mixing in numerical simulations of clouds and climate, interpretations of remote sensing measurements.

This paper constitutes the first in a series of three papers. It considers the final stage of mixing based on the formal definitions of homogeneous and extreme inhomogeneous mixing. These two types of mixing present two extreme regimes of mixing. The following two papers provide a detailed analysis of the time dependent processes during homogeneous (Pinsky et al., 2016a) and inhomogeneous (Pinsky et al., 2016b) mixing where non-extreme regimes are considered as well.

This paper is arranged in the following way. Section 2 presents analysis of the analytical relationship between N, $N\overline{D}$, β, q, D_v and mixing fraction μ for the cases of homogeneous and extreme inhomogeneous mixing. In Sect. 3 the obtained analytical relationships are compared with the numerical simulations of N, β, q, D_v formed at the final stage of mixing. Section 4 presents results of simulation of progressive mixing and its effect of the relationships between moments. Examples of relationship between N, β, q and D_v from in-situ observations are provided in Sect. 5. The discussion and concluding remarks are presented in Sect. 6 and 7.

2 Effect of mixing on microphysical variables

2.1 Phenomenological consideration

The conceptual diagrams of homogeneous and extreme inhomogeneous mixing are shown on Fig. 1. During the first stage of extreme inhomogeneous mixing the subsaturated parcel is engulfed into the cloudy environment (Fig. 1a1). Then, the droplets at the interface of the sub-saturated parcel and the cloud environment undergo complete evaporation until the air within the engulfed volume reaches saturation (Fig. 1a2). After that the saturated but droplet free parcel mixes with the rest of the cloud environment (Fig. 1a3). The result of inhomogeneous mixing is that the cloud parcel has reduced droplet concentration and the droplet sizes remain unchanged.

In the case of homogeneous mixing after entraining into a cloud (Fig. 1b1), the subsaturated parcel "instantly" mixes up with its cloud environment (Fig. 1b2) leading to undersaturation of the total volume. Then, all droplets throughout the mixed volume undergo simultaneous evaporation until the equilibrium state is reached. The result of homogeneous mixing is a cloud volume with reduced concentration of droplets and droplets with reduced sizes (Fig. 1b3).

Based on mass and energy conservation the final state of the bulk parameters (i.e. liquid water mixing fraction, humidity, temperature, etc.) is the same for both types of mixing. However, in the case of extreme inhomogeneous mixing saturation is reached through complete evaporation of some fraction of droplets, and their sizes remain constant. Whereas in case of homogeneous mixing saturation is reached through a uniform evaporation of droplets, and the total number of droplets remains unchanged. It should be noted, that in both cases the droplet concentration decreases due to dilution by the mixed droplet free sub-saturated parcel.

The following discussion will be specifically focused on the microphysical properties formed at the final stage of the homogeneous and extreme inhomogeneous mixing. The processes occurring during mixing state (i.e. transition 1a→2a and 1b→2b in Fig. 1) remain outside the frame of this work. Following the formalism of homogeneous and extreme inhomogeneous mixing, the process of mixing reaches the final stage when (1) the entrained and cloud environment are mixed up and the spatial gradients of the microphysical (N, β, q, etc.) and environmental (T, S, e, etc.) parameters approach to zero; (2) the diffusional process related to droplet evaporation comes into equilibrium. The second condition is completed when (a) the environment reaches saturation state, or (b) the entire population of droplets is completely evaporated, if the entrained air is sufficiently dry.

The above description of homogeneous and extreme inhomogeneous mixing is highly idealized. Actual in-cloud mixing does not occur as a sequence of discrete events (Fig.1) that individually come to equilibrium only to be followed by next discrete mixing events. But rather it is occurring

continuously on a cascade of different spatial and time scales. Broadwell and Breidenthal (1982) summarized the experimental evidence and proposed the following description of mixing in turbulent shear layers. Mixing takes place in a series of events. Two shear layers exchange mass by engulfing parcels from an opposite layer into localized zones. The initially large-scale filaments of the two gases break down towards smaller scales due to the action of turbulence. The turbulence stretches the interface between the gases and enhances the molecular diffusion across the increasing surface. The actual mixing of the engulfed volume is a molecular diffusion process that is most effective after the break down volumes reduce to the Kolmogorov viscosity scale. It is anticipated that the reaction of the ensemble of droplets is a combination of homogeneous and inhomogeneous mixing with domination of one type of mixing over the other depending on the characteristic spatial and time scales of the environment determined by turbulence, cloud microphysics, state parameters and stage of mixing.

2.2 Methodology

The foregoing discussion will be focused on mixing between saturated cloud parcels and out-of-cloud sub-saturated air. The cloud parcel contains droplets with average diameter $\overline{D}_1$, liquid mixing ratio q_1 and number concentration N_1. The initial temperature in the cloud parcel is T_1, relative humidity $RH_1 = 1$, where $RH = e/e_s(T)$ (the explanation of variable notations is provided in Table 1). The second parcel is droplet free ($N_2 = 0$), sub-saturated with initial relative humidity $RH_2 < 1$ and temperature T_2. The mixing occurs isobarically, i.e. $p = \text{const}$. At the final stage of mixing the temperature and humidity formed in the resulting parcel are T and RH (appendix A). The process of mixing is completed, when the mixed parcel reaches equilibrium due to the air saturation (i.e. $RH = 1$,) or due to the complete evaporation of droplets. In the latter case the final humidity is $RH \leq 1$. The effect of the vertical velocity and vertical travel on final T, RH, and q is not considered here, i.e. vertical velocity $u_z = 0$.

Without the loss of generality the masses of the cloudy and sub-saturated volumes prior to the mixing are assumed to have a unit masses, i.e. $m_1 = 1$ and $m_2 = 1$. The mixing process will be considered as mixing of μ fraction of the cloud parcel with $(1 - \mu)$ fraction of the second (sub-saturated) parcel. The mixing cloud fraction may vary within the range of $0 \leq \mu \leq 1$. Therefore, the mass of the resulting mixed parcel is equal to $m_1\mu + (1 - \mu)m_2 = 1$. This approach simplifies the

consideration of mixing and allows considering all possible proportions of the mixing of two volumes.

2.3 Effect of mixing on liquid water and temperature

The mixing ratio of liquid water q formed at the final stage of mixing is determined by the mass of the mixing cloud water μq_1 and amount of evaporated water required to saturate the newly formed mixed volume δq_m. The mass balance of liquid water for the mixing volume yields

$$q = \mu q_1 - \delta q_m \quad , \tag{1}$$

where

$$\delta q_m = \frac{c_p R_v T_{m0}^2}{L^2} \ln\left(\frac{1 + \frac{e_s(T_{m0}) R_a L^2}{p c_{pa} R_v^2 T_{m0}^2}}{1 + RH_{m0} \frac{e_s(T_{m0}) R_a L^2}{p c_{pa} R_v^2 T_{m0}^2}} \right) \cong -\frac{S_{m0}}{A_2} \tag{2}$$

is the mixing ratio of liquid water required to saturate 1kg of volume with temperature T_{m0} and humidity RH_{m0} (appendix A); T_{m0}, RH_{m0} and S_{m0}, are the temperature, relative humidity and supersaturation formed in the volume after instantaneous air mixing, but before droplets start evaporating (appendix A); $e_S(T_{m0})$ is saturation vapor pressure at temperature T_{m0}.

Eq. (1) is a non-linear function of μ, since T_{m0}, e_{m0} and thus δq_m depends on μ. Eq.(1) can be simplified, if $T_1 = T_2$. In this case $T_{m0} = T_1 = T_2$, and $e_S(T_{m0}) = e_S(T_1) = e_S(T_2)$. Given that, the expression under logarithm in Eq.(2) can be expanded in series resulting in (appendix B)

$$\delta q_m = (1 - \mu)\delta q^* , \tag{3}$$

where

$$\delta q^* = \frac{c_p R_v T_2^2}{L^2} \ln\left(\frac{1 + \frac{e_S(T_2) R_a L^2}{p c_{pa} R_v^2 T_2^2}}{1 + RH_2 \frac{e_S(T_2) R_a L^2}{p c_{pa} R_v^2 T_2^2}} \right) \cong -\frac{S_2}{A_2} \tag{4}$$

is the mixing ratio of liquid water required to saturate 1 kg of the entrained dry air with temperature T_2 and humidity RH_2. Substituting Eq.(3) in Eq.(1) gives

$$q = \mu q_1 - (1 - \mu)\delta q^* , \tag{5}$$

The value of δq^* does not depend on μ, and Eq. (5) is a simple linear function of μ. The comparisons with numerical simulations showed, that Eq.(5) provides accuracy within few percent, when the temperature difference $|T_1 - T_2| < 2$°C. Although, in many cases $|T_1 - T_2|$ may vary a wide range reaching 10°C or higher, clouds with $|T_1 - T_2| < 2$°C are quite common. Therefore, for the sake of simplicity, Eq.(5) and the assumption $T_1 \approx T_2$ will be used in the following consideration of mixing.

It should be noted that, Eqs (1) and (5) are valid for the cases, when $\mu > \mu_{cr}$. Here μ_{cr} is critical mixing fraction, which separates partial and complete evaporation of cloud water in the mixing volume (section 2.4). Cases when $\mu \le \mu_{cr}$ correspond to complete evaporation of droplets, and $q = 0$.

The temperature at the final stage of mixing can be estimated as (appendix C)

$$T = T_{m0} - \frac{(1-\mu)\delta q^* L}{c_{pa}}, \quad \text{when } \mu > \mu_{cr} \tag{6a}$$

$$T = T_{m0} - \frac{\mu q_1 L}{c_{pa}} \quad \text{when } \mu \le \mu_{cr} \tag{6b}$$

Eqs. (1), (5), (6) were obtained based on mass and energy conservation, and they do not depend on how mixing proceeds. Therefore, Eqs. (1), (5), (6) are valid for both homogeneous and inhomogeneous mixing.

2.4 Complete evaporation

As mentioned in section 2.2 the process of mixing is complete only after reaching equilibrium by saturating the mixed volume or by evaporating of all cloud droplets depending on the mixing fraction μ. The critical mixing fraction μ_{cr}, corresponding to evaporation of all droplets, can be found from Eq.(5) when $q = 0$, i.e.

$$\mu_{cr} = \frac{\delta q^*}{q_1 + \delta q^*} \tag{7}$$

Critical mixing fraction separates μ in two subranges: (a) $1 \ge \mu > \mu_{cr}$ where q is described by Eqs.(1) or (5) and $RH_m = 1$; (b) $\mu_{cr} \ge \mu \ge 0$ where $q = 0$ and $RH_m \le 1$.

For the general case when $T_1 \ne T_2$, μ_{cr}, can be found by solving the non-linear equation

$$\mu_{cr} q_1 - \delta q_m(\mu_{cr}) = 0 \tag{8}$$

Figure 2 shows comparisons of dependences of μ_{cr} vs. q_1 calculated from Eq. (7) and those deduced from a numerical model (Sect. 3). Critical mixing fraction μ_{cr} is also shown by black stars in Fig. 4. The locations of the stars in Fig.4 coincide well with the locations, where the modeled microphysical moments become zero. The obtained agreement between analytical and modeled μ_{cr} in Figs. 2 and 4 validates the developed approach.

2.5 Extreme inhomogeneous mixing

Within the framework of extreme inhomogeneous mixing some fraction of droplets undergo complete evaporation, whereas the rest of the droplets remain unchanged. Therefore, such a process results in scaling the droplet size distribution $f(D)$, i.e.

$$f(D) = k f_1(D) \tag{9}$$

where k is some coefficient dependent on μ and the initial environmental parameters of the mixing volumes, $f_1(D)$ is the droplet size distribution before mixing. Equation (9) yields relationships between pairs *n*th and *m*-th moments

$$\frac{M_n}{M_{n1}} = \frac{M_m}{M_{m1}} \tag{10}$$

where $M_n = \int_0^\infty f(D) D^n dD \Big/ \int_0^\infty f(D) dD$ is the *n*th moment of $f(D)$. Therefore, it is anticipated that for extreme inhomogeneous mixing droplet number concentration N (0th moment), extinction coefficient β (2nd moment), liquid water mixing ratio q (3rd moment), along with other moments, will correlate with each other, i.e.

$$\frac{N}{N_1} = \frac{\beta}{\beta_1} = \frac{q}{q_1} \tag{11}$$

One of the consequences of Eqs. (9)-(11) is that the characteristic droplet sizes $\overline{D}$, D_2, D_v, D_{eff} will remain constant during inhomogeneous mixing.

For the case $T_1 = T_2$ and $\mu > \mu_{cr}$ Eqs. (5) and (11) yield the dependence of N vs. μ

$$N = N_1 \left(\mu - \frac{(1-\mu)\delta q^*}{q_1} \right) \tag{12}$$

$$\beta = \beta_1 \left(\mu - \frac{(1-\mu)\delta q^*}{q_1} \right) \tag{13}$$

For a general case when $T_1 \neq T_2$ the term $(1-\mu)\delta q^*$ in Eqs. (12) and (13) should be replaced by $\delta q_m(\mu)$ (Eq.(2)).

2.6 Homogeneous mixing

For homogeneous mixing, when $\mu > \mu_{cr}$, the droplet number concentration changes only due to dilution by the entrained air, i.e.

$$\frac{N}{N_1} = \mu \tag{14}$$

Assuming $T_1 = T_2$, and substituting Eq. (5) in (14) yields:

$$\frac{N}{N_1} = \frac{q + \delta q^*}{q_1 + \delta q^*} \tag{15}$$

As follows from Eq. (15) N and q are linearly related for homogeneous mixing. However, no linear relationships exist between other moments. Thus, substituting the definition of the liquid water mixing ratio $q = \pi\rho_w N D_v^3/6\rho_a$ in Eq. (15) yields the relationship between mean volume droplet size, concentration and liquid water mixing fraction

$$\frac{D_v^3}{D_{v1}^3} = 1 + \left(1 - \frac{N_1}{N}\right)\frac{\delta q^*}{q_1} \tag{16a}$$

$$\frac{D_v^3}{D_{v1}^3} = \frac{q}{q_1}\left(\frac{q_1 + \delta q^*}{q + \delta q^*}\right) \tag{16b}$$

In a similar way the relationship between the extinction coefficient $\beta = Q\pi N D_2^2/4$, N and q can be written as

$$\frac{\beta}{\beta_1} = \frac{N}{N_1}\left(1 + \left(1 - \frac{N_1}{N}\right)\frac{\delta q^*}{q_1}\right)^{2/3} \tag{17a}$$

$$\frac{\beta}{\beta_1} = \left(\frac{q}{q_1}\right)^{2/3}\left(\frac{q + \delta q^*}{q_1 + \delta q^*}\right)^{1/3} \tag{17b}$$

In Eqs. (17a) and (17b) it is assumed that $D_2 \approx D_v$.

Substituting in Eq. (16) the expression for the time of phase relaxation $\tau_p = 1/bN\overline{D}$ (e.g. Squires 1952; Korolev and Mazin, 2003) and assuming $\overline{D} \approx D_v$ yields

$$\frac{\tau}{\tau_1} = \frac{N_1}{N}\left(1+\left(1-\frac{N_1}{N}\right)\frac{\delta q^*}{q_1}\right)^{-1/3} \quad (18)$$

For the cases when the temperature difference $|T_1 - T_2|$ exceeds a few degrees, the effect of μ on T_m and S_m should be taken into consideration in the calculations of evaporated water. For such cases δq_m (Eq. (2)) should be used instead of δq^*. Using Eq. (14) δq_m can be presented as a function of $\frac{N}{N_1}$, i.e. $\delta q_m(\mu) = \delta q_m\left(\frac{N}{N_1}\right)$. Replacing Eq. (5) by (1) in the above consideration, the equations Eqs. (15)-(18) can be rewritten as

$$\frac{N}{N_1} = \frac{q + \delta q_m\left(\frac{N}{N_1}\right)}{q_1} \quad (19)$$

$$\frac{D_v^3}{D_{v1}^3} = 1 - \frac{\delta q_m\left(\frac{N}{N_1}\right)}{q_1}\frac{N_1}{N} = \frac{q}{q + \delta q_m\left(\frac{q}{q_1}\right)} \quad (20)$$

$$\frac{\beta}{\beta_1} = \frac{N}{N_1}\left(1 - \frac{\delta q_m\left(\frac{N}{N_1}\right)}{q_1}\frac{N}{N_1}\right)^{2/3} = \frac{q^{2/3}\left(q + \delta q_m\left(\frac{\beta}{\beta_1}\right)\right)^{1/3}}{q_1} \quad (21)$$

$$\frac{\tau_p}{\tau_{p1}} = \frac{N_1}{N}\left(1 - \frac{\delta q_m\left(\frac{N}{N_0}\right)}{q_1}\frac{N_1}{N}\right)^{-1/3} \quad (22)$$

Eqs. (19)–(22) can be solved numerically.

2.7 Degenerate case

As follows from Eq.(5), if

$$\frac{(1-\mu)}{\mu}\frac{\delta q^*}{q_1} << 1 \quad (23)$$

then $q_1 \geq q \gg \delta q^*$. If the condition in Eq. (23) is satisfied, then the terms associated with δq^* in Eqs. (15)-(18) can be neglected. This results in correlation of all moments, i.e. $N/N_1 = \beta/\beta_1 = q/q_1$

297 (compare with Eq.(11)). This corresponds to the degenerate case, when the difference between the
298 homogeneous and inhomogeneous mixing vanishes. Thus, the dimensionless parameter $\xi = \frac{1-\mu}{\mu}\frac{\delta q^*}{q_1}$
299 in Eq.(23) can be used for characterization of proximity of the homogeneous mixing moments to
300 those formed during extreme inhomogeneous mixing.

301 The range of μ in ξ is limited by $\mu_{cr} < \mu \leq 1$, so that $0 < \frac{1-\mu}{\mu} \leq \frac{q_1}{\delta q^*}$. This gives the range of
302 changes of ξ, i.e. $0 \leq \xi \leq 1$ for the mixing without complete evaporation of all droplets. The
303 degenerate case corresponds to $\xi \to 0$, whereas $\xi \to 1$ corresponds to maximum difference of the
304 moments for homogeneous and extreme inhomogeneous mixing.

305 As follows from Eqs. (4) and (23) approaching to the degenerate case ($\xi \to 0$) occurs, when one
306 of the following conditions or their combination is satisfied: (a) $RH_2 \to 1$; (b) $E_s(T) \to 0$ at low
307 temperatures; (c) $q_1 \gg \delta q^*$; (d) $\mu \to 1$. The effect of RH, T, q_1 and μ on mixing will be demonstrated
308 in Sect.3.

309 Figure 3 shows dependence of ξ vs. μ. The grey area in Fig.3 indicates the region where
310 identification of type of mixing from in-situ measurements (Sect.5) may be hindered due to proximity
311 of the moments for homogeneous and extreme inhomogeneous mixing. Thus for $\delta q^*/q_1$ =0.01
312 identification of type of mixing is ambiguous for nearly the entire range of μ.

313 For the general case, when $T_1 \neq T_2$, it should be $\xi = \frac{|\delta q_m(\mu)|}{\mu q_1}$. An absolute value $|\delta q_m(\mu)|$
314 should be used in ξ since $\delta q_m(\mu)$ can be negative (Appendix A, Fig.A1), if mixing results in
315 supersaturation Sect. 3.4).

316 The coefficient ξ may be useful for identification type of mixing from in-situ observations. It is
317 worth nothing, that the ratio $\frac{\delta q^*}{q_1} \cong \frac{S_2}{A_2 q_1}$ is equal to the parameter R (Pinsky et al. 2016ab), which
318 plays an important role in determining scenarios of droplet evaporation in turbulent environment.
319

320 **3 Comparisons with numerical simulations**

321 Numerical simulations were performed to examine accuracy and limitations of the analytical
322 expressions in Sect.2 and to conduct a sensitivity test to environmental and cloud parameters. The
323 simulations have been performed with the help of a parcel model similar to that in Korolev (1995).
324 The ensemble of droplets in the simulation was assumed to be monodisperse. For the case of extreme
325 inhomogeneous mixing the amount of evaporated water Δq required to saturate the mixed volume

was calculated first. If $\Delta q < \mu q_1$, then the concentration of evaporated droplets was calculated as $N_{ev} = \frac{\Delta q}{m_d}\rho_a$, where $m_d = \pi\rho_w D^3/6$. Then, the concentration of the remaining droplets $N = N_1 - N_{ev}$ was recalculated based of the calculation on the volume formed after mixing. If $\Delta q \geq \mu q_1$, then all droplets evaporate, and $N = 0$.

For the case of homogeneous mixing in the first step the engulfed parcel instantly mixes with the cloud parcel resulting in a new humidity RH_{m0}, temperature T_{m0} and volume V_{m0}. After that the droplets start evaporating until either their complete evaporation or saturation over liquid is reached. The calculations stopped when, either $D < 0.2$μm or $(E_S - e)/E_S < 0.001$, respectively.

3.1 Effect of mixing fraction

Figure 4 shows the results of the simulation of different moments and state parameters vs. μ. The calculations were performed for different relative humidity of the entrained parcel RH_2 = 0.2, 0.5, 0.8 and 0.95. As seen from Fig.4 for the case of homogeneous mixing only N and q are linearly related with μ, the rest of the variables have non-linear dependences on μ. For the case of extreme inhomogeneous mixing all $f(D)$ moments and droplet sizes linearly depend on μ. Note, for $\mu \leq \mu_{cr}$ all moments are equal to zero.

Since the amount of the evaporated liquid water does not depend on the type of mixing, the dependences of $q(\mu)$ are the same for both homogeneous and inhomogeneous mixing (Fig.4a). The type of mixing has the most pronounced effect on the droplet concentration (Fig.4b) and droplet sizes (Fig.4e).

Figure 4g shows the dependences RH_{m0} and RH vs. μ. Here RH_{m0} is the relative humidity at the initial stage of homogeneous mixing before droplets start evaporating (Fig. 1b2). Figure 3h presents comparisons of modeled $T(\mu)$ and those calculated from Eqs.(6a,b) and (C4). The independence of $q(\mu)$, $RH(\mu)$ and $T(\mu)$ on type of mixing (Fig.4a,g,h) is the consequence of the mass and energy conservation, which are not contingent on type of mixing.

3.2 Effect of humidity of entrained air

The diagrams in Fig. 5a-c show the dependences of normalized β, q and D_v vs. N/N_1 calculated from numerical simulations and analytical equations from Sect. 2. The calculations were performed for different humidity of the entrained air RH_2. As seen from Fig. 5a-c, the normalized dependences

for homogeneous mixing $q(N)$, $\beta(N)$ and $D_v(N)$ tend to approach the line of extreme inhomogeneous mixing when relative humidity RH_2 approaches to 1. This is consistent with the degenerate case, when $\xi \to 0$ (Sect.2.7). In this case droplets behave as a passive admixture, and they do not interact with the environment.

3.3 Effect of liquid water mixing ratio

Figure 5d-f demonstrate the sensitivity of $q(N)$, $\beta(N)$ and $D_v(N)$ to liquid water mixing ratio q_1. It is seen, that the increase of q_1 results in $q(N)$, $\beta(N)$ and $D_v(N)$ (calculated for homogeneous mixing) approaching towards $q(N)$, $\beta(N)$ and $D_v(N)$ for the inhomogeneous mixing. In other words, the sensitivity of the microphysical parameters to the type of mixing increases with the decrease of q_1. From a practical viewpoint it means, that from in-situ observations the difference between homogeneous and inhomogeneous mixing is anticipated to be more pronounced for the cases with a relatively low liquid water mixing ratio (e.g. q_1<1g/kg). Such behaviour is consistent with the consideration in Sect. 2.7.

3.4 Effect of temperature, case $T_1 = T_2$

Figure 5g-j shows the effect of temperature on the normalized $q(N)$, $\beta(N)$ and $D_v(N)$ for $T_1 = T_2$. Figure 5g-j indicate that the difference between the moments becomes most pronounced at warm temperatures, whereas at cold temperatures (e.g. T= -30^{O}C), $q(N)$, $\beta(N)$ and $D_v(N)$ for homogeneous mixing are approaching those for the extreme inhomogeneous mixing limit.

Such behavior is explained by the fact that liquid water deficit δq_m decreases with decreasing temperature (appendix A, Fig. A1). At low temperatures (T=-30^{O}C) the amount of evaporated water δq_m is so small, that homogeneous mixing with dry out-of-cloud air will have approximately the same effect as mixing with saturated air (i.e. degenerate case, Sect. 2.7).

Overall, as follows from Fig.5 the results the analytical predictions (Sect. 2) turned out to be in a good agreement with numerical simulations.

3.5 Effect of temperature, case $T_1 \neq T_2$

Isobaric mixing of two nearly saturated volumes with $T_1 \neq T_2$ may result in supersaturated environment (e.g. Rogers, 1976; Bohren and Albrecht, 1998). Mixing resulting in supersaturation is different in principle from the mixing with evaporating droplets. In this case the meaning of

387 homogeneous and inhomogeneous mixing becomes ambiguous. Formation of supersaturation leads
388 to different dependences between $N\overline{D}$, β, q, $\overline{D}$ and N as compared to those shown in Figs. 3–4, when
389 $T_1 = T_2$.

390 Figure 6 presents a set of diagrams similar to those in Fig.4, but calculated for the cases when
391 $T_1 \leq T_2$. It turns out that for the case of extreme inhomogeneous mixing the temperature difference
392 between T_1 and T_2 breaks down linear dependences of the microphysical moments (e.g. $N\overline{D}$, β, q
393 Fig. 6a,c,d) vs. μ .

394 Figure 7 presents the effect of the temperature difference ΔT on the normalized dependences
395 $q(N)$, $\beta(N)$ and $D_v(N)$. In clouds, high supersaturation resulting from isobaric mixing may lead to
396 activation of interstitial CCN, which may increase N and decrease D_v (Korolev and Isaac, 2000).
397 However, no activation of new droplets during isobaric mixing was allowed in this study. For the
398 cases when $RH_{m0} > 1$ (Fig. 7, AB on line 1) the condensed water was uniformly distributed between
399 available droplets. Therefore, $q(N)$, $\beta(N)$ and $D_v(N)$ calculated for homogeneous and extreme
400 inhomogeneous mixing coincide with each other on this interval.

401 Numerical simulations also showed, that the effect of temperature on mixing is more pronounced
402 for the cases, when the cloud temperature is warmer than that of the entrained air, i.e. $T_1 > T_2$, as
403 compared to the cases with $T_1 < T_2$.

404

405 **4. Progressive mixing**

406 **4.1 Effect on microphysical parameters**

407 In the previous sections the mixing was considered as a single event, i.e. μ fraction of the cloudy
408 air mixed up with $(1-\mu)$ fraction of entrained dry air. Such mixing will be referred to as "primary"
409 mixing. Primary mixing results in an ensemble of elementary volumes characterized by a set of
410 microphysical and state parameters i.e. $D_v(\mu)$, $N(\mu)$, $RH(\mu)$, $T(\mu)$, etc. Each of these parameters
411 has a functional dependence on μ, and what is important, these parameters have functional
412 relationships between each other.

413 In reality mixing is a continuous process. It does not stop after the primary mixing. The
414 elementary volumes formed after primary mixing continue to progressively mix with each other.

415 The second stage of mixing will result in an ensemble of elementary volumes characterized by
416 a set of parameters $D_v^{(2)}$, $N^{(2)}$, $RH^{(2)}$, $T^{(2)}$, etc. Here the superscript $^{(2)}$ indicates the stage of mixing.
417 After the second stage the mixed volumes undergo subsequent stages of mixing.

418 The idealised conceptual diagram of the progressive mixing is shown in Fig. 8. Each stage of
419 mixing results in an ensemble of elementary parcels formed for different $\mu_j^{(n)}$. The elementary
420 parcels continue mixing with each other and cloud environment during the subsequent mixing stages.
421 As mentioned in Sect. 2.1, the actual process of mixing is indeed much more complex than the
422 sequence of discrete events portrayed in Fig.8. However, as it will be shown below, this simplified
423 consideration of allows establishing main features of evolution of relationships between the
424 microphysical moments affected by mixing. The obtained results facilitate identification of type of
425 mixing from in-situ measurements.
426 Progressive homogeneous mixing was simulated with the help of a numerical model, where
427 parcels were randomly mixed with each other and with the cloud environment. The mixing fraction
428 μ was also set to be random during each mixing event. Models of stochastic mixing have been used
429 in a number of studies (e.g. Krueger et al., 1997; Su et al., 1998; Burnet and Brenguier, 2007). In the
430 present work the analysis of progressive mixing is expanded to examine its effect on the relationship
431 between moments of the droplet size distribution.
432 The results of the progressive homogeneous mixing for the first four stages are presented in Fig.
433 9. As seen from Fig. 9 the functional relationship between the pairs of microphysical and state
434 parameters exists only for the primary stage. For higher mixing stages these functional relationships
435 break down. Thus, cloud volumes with the same $N^{(2)}$ may have different $D_v^{(2)}$. Figure 9 also shows
436 that the regions of scattering of $q(N)$, $\beta(N)$ and $D_v(N)$ for stages 2, 3 and 4 are limited from above
437 by the inhomogeneous mixing (red dashed lines) and from below by primary homogeneous mixing
438 (red solid lines).
439 Figure 10 presents a conceptual $N-q$ diagram explaining breaking the functional relationships
440 during progressive homogeneous mixing. After the first stage of mixing the $N-q$ points will be
441 scattered along the line OB and point C. The line OB corresponds to the ensemble of points with
442 $RH=1$. Therefore, result of mixing between two saturated volumes randomly selected on AB, will
443 remain on the same line. Point C corresponds to the ensemble of points with $N=0$, $RH_2 \leq$
444 $RH_C\left(\mu^{(1)}\right) \leq 1$, where $0 \leq \mu^{(1)} < \mu_{cr}$. Therefore, mixing between point A (Fig.10) and point C,
445 when $RH=1$ will result in scattering along the line AC (degenerate case). Points resulted from
446 mixing between A ($RH=1$) and point C, when $RH_2 \leq RH_C < 1$, will scattered over the ensemble
447 of dashed lines shown in Fig.10. These lines will fill the sector CAB. Random mixing between points

448 on the line OB and C, will eventually fill the entire sector COB. The same consideration can be
449 applied to progressive mixing between other moments.

450 During the progressive mixing $N^{(n)}$, $\beta^{(n)}$, $q^{(n)}$ and $D_v^{(n)}$ formed in the elementary parcels tend
451 to approach those in the undiluted cloud, i.e. N_1, β_1, q_1 and D_{v1}. This process can be considered as
452 a surrogate to the diffusion process between the cloud and sub-saturated out-of-cloud environment.
453 The convergence of $\beta^{(n)}$, $q^{(n)}$ and $D_v^{(n)}$ during the progressive mixing can be seen in Fig. 9, where
454 the scattering of normalized $q^{(n)}(N)$, $\beta^{(n)}(N)$ and $D_v^{(n)}(N)$ becomes denser towards the top-right
455 corner (1,1) with the increase of the stage of mixing.

456 It is worth noting that progressive mixing with the dry air only does not break the functional
457 relationships between the moments. This case is equivalent to detrainment of cloudy environment
458 into dry air. It can be shown that Eq.(14) remain valid at any stage of progressive homogeneous
459 mixing with dry air only, i.e. $N_j/N_1 = \mu^{(1)} \cdots \mu^{(n-1)}\mu^{(n)}$ where $\mu^{(n)}$ is the mixing fraction at the n-
460 th stage of mixing. Eqs. (15)-(24) also remain valid for the progressive mixing with the dry air only.

461 As follows from Eq. (9) for the case of extreme inhomogeneous mixing the progressive mixing
462 does not affect the functional relations between $N^{(n)}$, $\beta^{(n)}$, $q^{(n)}$ and $D_v^{(n)}$ and other microphysical
463 parameters. These relations remain the same regardless of the actual stage of mixing. This is one of
464 the fundamental differences between homogeneous and extreme inhomogeneous mixing, which can
465 be used for identification of type of mixing from in-situ measurements.
466
467 **4.2 Effect on droplet size distributions**

468 Figure 11 shows modeled droplet size distributions averaged over the ensembles of elementary
469 volumes corresponding to the first four stages of homogeneous mixing. As seen from Fig. 11a–d for
470 the case with $T_1 = T_2$ the droplet size distributions are broadened towards small sizes. Depending on
471 the stage of mixing and mixing fraction μ the size distributions formed in each elementary volume
472 may be unimodal or multimodal. However, due to the random nature of the modal sizes formed
473 during mixing, the average size distributions become smooth and unimodal (Fig.11a-d).

474 Broadening of droplet size distributions towards small sizes during homogeneous mixing is well
475 known and it was demonstrated in a number of studies (e.g. Baker and Latham, 1982; Jensen and
476 Baker, 1989; Jeffery, 2007; Kumar et al., 2013). However, if mixing results in supersaturation
477 (section 3.4), then the droplet size distribution may broaden towards larger sizes (Fig. 11e–h). For

this to occur, both the temperature difference between the cloud and the environment $|T_1 - T_2|$ and the relative humidity of the environment RH_2 must be sufficiently large. Such conditions are inherently unstable, however, this might occur in regions that have been moistened through prior cloud detrainment. Thus homogeneous mixing may result in broadening of droplet size distributions towards either smaller or larger sizes (Fig.11).

These results were obtained in the frame of the formalism of homogeneous and inhomogeneous mixing. The following two works in this series (Pinsky et al., 2016a, b) will discuss the broadening of polydisperse and monodisperse $f(D)$ during both homogeneous and inhomogeneous mixing in greater details.

5 Identification of type of mixing from in-situ observations

The purpose of this section is to attempt identifying type of mixing based on examining relationships between basic microphysical parameters N, β, LWC, D_v measured from in-situ.

5.1 Expected relationships between the moments

Prior proceeding with the analysis of in-situ data we summarize the results of the previous consideration on how homogeneous and extreme inhomogeneous mixing is expected to manifest itself in relationships between basic microphysical parameters, such as N, β, q and D_v.

For extreme inhomogeneous mixing the relationship between the pairs of N, β and q are determined by linear dependences $M_n = \alpha_{nm} M_m$ (Eq. 10) at any stage of mixing. As follows from Eq. (11) the slopes α_{nm} for $q(N)$, $\beta(N)$ and $q(\beta)$ are equal to the ratios q_1/N_1, β_1/N_1, and q_1/β_1, respectively, where N_1, β_1 and q_1 correspond to undiluted adiabatic values. The values of N_1, β_1 and q_1 may vary depending on the location inside the cloud and environmental conditions at the cloud base. Thus, the adiabatic value of q_1 is a function of elevation above the cloud base ΔZ, whereas N_1 depends on the vertical velocity at the cloud base u_z and the aerosol load. Therefore, the scattering of $q - N$ points will be aligned along an ensemble of different lines determined by q_1/N_1, which are specific to different cloud volumes. The conceptual diagram of the scattering of $q - N$ measurements in a cloud with extreme inhomogeneous mixing is shown in Fig. 12a. The scatter diagrams for other moments (e.g. $q - \beta$, $N - \beta$) will have the similar patterns as that in Fig. 12a.

For the case of homogeneous mixing the functional relationship between the pairs of N, β, q and D_v are disrupted by a progressive mixing. As shown in Sect. 4.1 the ensemble of points of N, β and q will be scattered within a sector, which is limited by lines determined by Eq. (11) (extreme

inhomogeneous mixing) and Eqs. (15)-(17) (primary homogeneous), respectively (Fig. 9). What is important, is that the top of the sectors for $q(N)$ and $\beta(N)$ correspond to points $[N_1, q_1]$ and $[N_1, \beta_1]$, respectively. Since N_1, β_1 and q_1 may vary within the same cloud, it is anticipated that the N, β and q measurements will be scattered within an ensemble of sectors as shown in Fig. 12b.

It is important to note that that during homogeneous mixing prior reaching equilibrium, functional relationships between the microphysical moments do not exist either. After the instant mixing of cloud fraction μ with entrained air (Fig. 1b(2)), $q_{m0} = \mu q_0$ and $N_{m0} = \mu N_0$. This state corresponds to point D in Fig.10. After that droplets start evaporating until liquid mixing ratio reaches point A (Fig.10), which corresponds to the equilibrium state ($RH = 1$). Therefore, during evaporation time $q - N$ points will be scattered along the line AD. Since, point D can be located anywhere on OC, the ensemble of $q - N$ points corresponding to non-equilibrium state will fill the COB area.

Thus, the absence of the functional relationships between the moments during homogeneous mixing may occur both during progressive mixing and during primary mixing prior reaching the equilibrium state. The evaporation time required to reach equilibrium during homogeneous mixing is discussed in details in Pinsky et al. (2016b), and it is usually limited by few tens of seconds. However, progressive mixing is not limited in time. Therefore, it is very likely that no functional relationship between microphysical parameters will be observed during in-situ measurements.

Fig.12 demonstrated a fundamental difference in scattering of $q - N$ for homogeneous and extreme inhomogeneous mixing, which will be used to facilitate identification of type of mixing in the following section.

5.2 Results of observations

The measurements were obtained on the University of Wyoming King Air aircraft during the COPE-MED project in South-Western part of UK during July-August 2013 (Leon et al., 2016). The UW King Air was equipped with a suite of microphysical instruments, including a DMT Cloud Droplet probe (CDP), designed for measurements of droplet sizes and their concentrations in the nominal size ranges 1–50 μm.

Figure 13 shows a time series of droplet concentration, extinction coefficient, liquid water content and mean volume droplet diameter measured by the CDP during transit through a convective cell on 18 July 2013. The CDP data were sampled at 10Hz, which corresponds to approximately 10m

spatial averaging. Visual examination of the spatial changes of N, β and LWC shows strong correlation. The amplitude of changes of these parameters reaches nearly one hundred percent with respect to their maximum. Contrary to that, the spatial variations of $\overline{D}$ and D_v are quite conservative and their values remain nearly constant. With the exception of two cloud holes between 13:50:42 and 13:50:44, the amplitude of fluctuations of D_v does not exceed 8% with standard deviation of 2.2%.

Figure 14 shows scatter diagrams of $LWC(N)$, $\beta(N)$, $LWC(\beta)$ and $D_v(N)$ measured by the CDP during seven consecutive penetrations of the same convective cell extended over a period of approximately 19 min. One of these penetrations is shown in Fig. 13. The measurements were conducted at H = 5500m and T = -12ºC. The relative humidity of the ambient air was approximately 20 %. At the beginning of the sampling no precipitation size particles were observed in the cloud. However, by the end of the sampling period some raindrops and ice crystals were present in the cloud. Despite the presence of some precipitation size particles, the scatter diagrams in Fig. 14a, b and d demonstrate high correlation between pairs N, β and LWC. The mean volume diameter in Fig. 14c shows very little changes from 19 to 17 μm, when concentration changes from 1100 to 500 cm^{-3}, However, for N < 200 cm^{-3}, the volume diameter decreases to 12–15 μm.

Red lines in Fig. 14 indicate $q(N)$, $\beta(N)$, $LWC(\beta)$ and $D_v(N)$ calculated for the 1st stage of homogeneous mixing. The calculations were performed for a monodisperse $f(D)$ with D_1=18.5μm, N_1 = 1100 cm^{-3}, and state parameters as during the measurements. Comparisons of dependences $q(N)$, $\beta(N)$, $LWC(\beta)$ and $D_v(N)$ based on in-situ measurements with those obtained from numerical simulations of homogeneous mixing show minor difference for high concentrations 700 cm^{-3}< N < 1100 cm^{-3} (Fig. 14a–c). Simulation also shows that for this specific case the difference between homogeneous and inhomogeneous mixing does not exceed 10% when 700 cm^{-3}< N < 1100 cm^{-3}. Such difference remains within the errors of measurements. Therefore, in this specific cloud for the regions with N > 700 cm^{-3} the type of mixing cannot be unambiguously identified from the analysis of the dependences $LWC(N)$, $\beta(N)$, $LWC(\beta)$ and $D_v(N)$. This is consistent with the assessment of feasibility of segregation of homogeneous and inhomogeneous mixing in Fig.3 (dashed line). Since for homogeneous mixing $\mu = \frac{N}{N_1}$ (Eq.(14)), then assuming N_1 =1100cm^{-3}, Fig.3 suggests good separation of the moments for $N < 700$ cm^{-3}.

For the regions with N < 500 cm^{-3} the deviation between homogeneous mixing simulations and in-situ measurements in Fig.14 becomes well pronounced, and it extends beyond possible errors of

measurements. This suggests that the mixing in these regions is dominated by the extreme inhomogeneous type.

Figure 15 shows the same type of diagrams as in Fig. 14, which were measured during 45 consecutive traverses through an ensemble of deep convective cells. The sampling altitude varied in the range 3000m< H < 4500m, temperature -11ºC< T < 0ºC, relative humidity in the vicinity of clouds 15%< RH< 65 %. The cloud measurements were extended over a period of 2 h 13 m, which is suggestive that the convective cells were sampled at different stages of their lifetime. At the sampling level the concentration of raindrops varied from zero to few per liter, and their diameter did not exceed 2mm.

What is interesting that the scattering of $LWC(N)$, $\beta(N)$ and $LWC(\beta)$ (Fig. 15a, b and d) is limited by the sector, which originates from the zero point as in Fig.12a. Analysis of the measurements showed that the data points $LWC(N)$, $\beta(N)$, $LWC(\beta)$ in each individual cloud traverse are well aligned along the lines with different slopes (e.g. Fig.14). After averaging over the ensemble of clouds, the area of the scattered points turned out to be located inside a sector limited by the lines with smallest and largest slopes.

Comparisons of the scatterdiagrams $LWC(N)$, $\beta(N)$ and $LWC(\beta)$ in Figs.14 and 15 with the conceptual diagrams in Fig.12 unambiguously suggest that interaction between cloud and environment in the studied clouds was dominated by inhomogeneous mixing. It should be emphasized that analysis of a stand alone mixing diagram $N - D_v$ would not allow unambiguously draw such conclusion.

6. Discussion

One of the assumptions in most past studies is that for a sequence of the cloud samples collected along the flight path, the adiabatic values of N_1, q_1, β_1, D_1 and environmental parameters e_2 and T_2 remain the same. In fact these parameters may vary both within the same cloud or sequence of samples clouds, and the amplitude of their variations depends on microphysical and thermodynamical properties inside and outside the cloud environment. This variation will result in an ensemble of relationships $M_n = F_{nk}(M_k)$, and enhance scattering of the data points. In such cases identification of the type of mixing based on the $N - D_v$ diagram may result in confusion between homogeneous and inhomogeneous mixing. As demonstrated in Sect. 5, consideration of $N - q$ and $N - \beta$ diagrams may provide a better identification type of mixing.

Strictly speaking the identification of type of mixing from particle probe measurements as it was performed in Sect. 5 is incomplete. It allows establishing correlation between microphysical moments and makes a formal conclusion about the mixing type, however it does not allow judgement about stage of mixing (i.e. whether mixing is complete by reaching equilibrium). In most previous studies, including this one, identification of type of mixing was based on the assumption that the sampled cloud volume is in equilibrium state ($RH = 1$), and that it reached the final stage of mixing (Fig.1 a2, a3, b3). It is possible that at the moment of measurement the process of mixing is not complete and the droplet free filaments remained undersaturated (Fig.1 a1, b1, b2). In this case the relationship between different moments may be well described as $M_n = \alpha_{nk} M_{nk}$ and the mixing be confused with inhomogeneous mixing.

In order to identify stage of mixing, high frequency collocated measurements of temperature and humidity are required. Unfortunately, current technology does not allow such measurements yet.

The basic assumption underlying the analysis of relationships between moments is that the cloud environment is not affected by other non-adiabatic processes. Thus, collision-coalescence, riming or Wegener-Bergeron-Findeisen processes may change the droplet number concentration and liquid water content, and therefore, affect the relationship between the moments. Activation of interstitial CCN will result in breaking correlation between the moments due to formation of large concentration of droplets. Broad size distributions may also hinder identification of type of mixing due to partial evaporation of small droplets (Pinsky et al. 2016a)

It is anticipated that most suitable candidates to study mixing-entrainment process are non-precipitating convective clouds and stratocumulus clouds with relatively narrow droplet size distributions.

Another limiting factor is that the above consideration did not account for the effect of changing relative humidity in a vertically ascending parcel. Thus in droplet free entrained air RH increases approximately 10% for $\Delta z = 200$m at T = 0 ^{o}C. After reaching saturation the mixing turns into a degenerate case, which will appear as extreme inhomogeneous mixing. Joint effects of evaporating droplets and an increase in RH during the vertical ascent may facilitate reaching saturation state. This case may also be relevant to the convective cloud described in Sect.5.2.

633 **7. Conclusions**

634 This study analyzes dependences of different moments of $f(D)$ in the frame of formalism of
635 homogeneous and extreme inhomogeneous mixing. The analysis was performed for the final stage
636 of mixing based on the mass and energy conservation consideration. The following results were
637 obtained in the frame of this study:

638 1. Simple analytical relationships between the main microphysical moments were obtained for
639 the final state homogenous and extreme inhomogeneous mixing.

640 2. It was shown that the functional relationships between the moments exist only for the first
641 stage of homogeneous mixing, when equilibrium is reached. Subsequent progressive homogeneous
642 mixing breaks the functional relationship between the moments.

643 3. It was demonstrated that consideration of scattering $N - LWC$, $N - \beta$ diagrams facilitates
644 identification of type of mixing from in-situ measurements. For extreme inhomogeneous mixing the
645 scattering of the data points $N - LWC$, $N - \beta$ will be limited by a sector originating at zero point
646 (Fig.12a). However, for homogeneous mixing the scattering data points will be limited by a sector
647 originating at (N_1, LWC_1) and (N_1, β_1) (Fig.12b). Utilizing a stand-alone conventional $N - D_v$
648 mixing diagram may not provide unambiguous answer about type of mixing.

649 4. The developed approach was applied to a set of in-situ measurements collected in convective
650 clouds. The analysis of the dependences between N, β, LWC and D_v suggests that the interaction
651 between entrained and cloudy environments for the studied clouds was dominated by
652 inhomogeneous mixing.

653 The present study considers relationships between different moments of $f(D)$ for the final stage
654 of mixing. The following two works Pinsky et al. (2016a, b) in this series provide a detailed analysis
655 of time dependences of droplet size distributions and its moments during homogeneous and
656 inhomogeneous mixing.

657

658 *Acknowledgement.* The authors appreciate two anonymous reviewers for their comments. Alexei
659 Korolev work was supported by Environment Canada and Transport Canada. The COPE-MED
660 project was funded by National Science Foundation grant AGS-1230292 and AGS-1230203. The
661 contribution of Mark Pinsky and Alex Khain was supported by the Israel Science Foundation (grant
662 1393/14), the Office of Science (BER), US Department of Energy Award DE-SC0006788 and the
663 Binational US-Israel Science foundation (grant 2010446).

Appendix A: Liquid water deficit

The objective of this section is to find the amount of liquid water, which is required to be evaporated in order to saturate the parcel formed after mixing. Assume that q_{v1}, q_{v2} are the mixing vapor ratios in the cloudy and entrained parcels, respectively, and T_1, T_2 are their respective initial temperatures. First, we find the saturation ratio S_{m0} formed after instant mixing of the cloud and entrained before the cloud droplets start evaporating.

The vapor mixing ratio q_{vm} formed in the mixed volume will be

$$q_{vm} = \mu q_{v1} + (1-\mu) q_{v2} \tag{A1}$$

The vapor pressure e_m in the mixed volume can be derived from Eq. (A1) by substituting $q_v = \frac{e}{p-e}\frac{R_a}{R_v}$, i.e.

$$e_m = p\frac{\mu + \frac{e_2(p-e_1)}{p(e_1-e_2)}}{\mu + \frac{(p-e_1)}{(e_1-e_2)}} \tag{A2}$$

The temperature of the mixed volume T_{m0} can be found from the energy conservation law

$$\mu(q_{v1}c_{pv} + c_{pa})(T_1 - T_{m0}) = (1-\mu)(q_{v2}c_{pv} + c_{pa})(T_{m0} - T_2) \tag{A3}$$

here c_{pv}, c_{pa}, are the specific heat capacitance of water vapor and dry air at constant pressure, respectively. Substituting q_{v1}, q_{v2} yields the temperature in the mixed volume

$$T_{m0} = \frac{\mu T_1 + \alpha(1-\mu)T_2}{\mu + \alpha(1-\mu)} \tag{A4}$$

here

$$\alpha = \frac{1 + \frac{c_{pv}R_a e_2}{c_{pa}R_v(p-e_2)}}{1 + \frac{c_{pv}R_a e_1}{c_{pa}R_v(p-e_1)}} \tag{A5}$$

With a good accuracy $\alpha \cong 1$. The resulting relative humidity after mixing the two volumes will be

$$RH_{m0} = \frac{e_{m0}}{e_S(T_{m0})} \tag{A6}$$

where $e_S(T_{m0})$ is the saturated vapor pressure at temperature T_{m0}.

The process of evaporation is accompanied by changing humidity and temperature due to latent heat of vaporization. This process is described by the Eq. (C2) in Korolev and Mazin (2003). Assuming the process to be isobaric (i.e. vertical velocity $u_z = 0$) and absence of ice ($dq_i = 0$), Eq. (C2) (Korolev and Mazin, 2003) yields

$$\frac{dS}{S+1} = \left(\frac{1}{S+1} \frac{pR_v}{e_S R_a} + \frac{L^2}{c_{pa} R_v T^2} \right) dq \qquad \text{(A7)}$$

Integrating Eq. (A7) from initial S_{m0} to saturation state, when $S = 0$, and taking into account that $RH = S + 1$, gives

$$\delta q_m = -b \ln\left(\frac{1 + aRH_{m0}}{1+a} \right) \qquad \text{(A8)}$$

the mixing ratio of liquid water required to evaporate in order to saturate 1kg of the cloud volume formed after mixing with the entrained air, but before droplet start evaporating. Here $a = \frac{E_S R_a L^2}{p c_p R_v^2 T_{m0}^2}$, $b = \frac{c_p R_v T_{m0}^2}{L^2}$.

Rewriting the right side of Eq.(A8) as $-b\ln\left(1 + \frac{a(RH_{m0}-1)}{1+a}\right)$, and taking into account that $\left|\frac{a(RH_{m0}-1)}{1+a}\right| < 1$, Eq.(A8) can be simplified as

$$\delta q_m = ab \frac{1 - RH_{m0}}{1+a} = -\frac{S_{m0}}{A_2} \qquad \text{(A9)}$$

where $A_2 = \frac{ab}{1+a}$. The analysis of Eqs. (A8)-(A9) shows that for wide range of temperatures -30 ^{o}C< T < 30 ^{o}C, both equations hold with high accuracy as long as the temperatures of the sub-saturated and cloud parcels $|T_1 - T_2| < 10^o$C.

Figure A1 shows comparisons of modeled δq_m and that calculated from Eqs. (A8) and (A9) for three different temperatures. The model solved a system of differential equation with incremental evaporation of liquid water until saturation is reached. As seen from Fig. A1 the agreement between modeled δq_m and that calculated from Eqs. (A8)-(A9) is quite good and does not exceed few percent at $RH_{m0} = 0.5$. This discrepancy results from assumption that e_S and T are constant in Eqs.(A8)-(A9).

Appendix B: Liquid water deficit when $T_1 = T_2$

712 Eq.(A2) by assuming that $p \gg e_1$ and $p \gg e_2$ can be simplified as

713 $$e_{m0} = \mu e_1 + (1-\mu)e_2 \quad \text{(B2)}$$

714 As follows from Eq.(A4) for the case $T_1 = T_2$ with high accuracy $T_{m0} = T_1 = T_2$. Therefore,
715 $e_S(T_{m0}) = e_S(T_1) = e_S(T_2)$. Dividing Eq.(B1) by e_S yields

716 $$RH_{m0} = \mu RH_1 + (1-\mu)RH_2 \quad \text{(B3)}$$

717 In most liquid clouds $RH_1 = 1$ (Korolev and Mazin 2003). Therefore, Eq.B2 turns into

718 $$RH_{m0} = \mu + (1-\mu)RH_2 \quad \text{(B4)}$$

719 Substituting Eq.(B4) in Eq.(B1) yields

720 $$\delta q_m = -b \ln\left(1 + \frac{a(1-\mu)(RH_2 - 1)}{1+a}\right) \quad \text{(B5)}$$

721 The expression under logarithm can be presented as the first two terms of the series expansion
722 of $\left(1 + \frac{a(RH_2-1)}{1+a}\right)^{(1-\mu)}$. Substituting this expression into Eq.(B5), gives

723 $$\delta q_m = (1-\mu)\delta q^* \quad \text{(B6)}$$

724 where

725 $$\delta q^* = -b \ln\left(\frac{1 + aRH_2}{1+a}\right) \quad \text{(B7)}$$

726 is the mixing ratio of liquid water required to saturate 1 kg of the entrained dry volume.

727

728 **Appendix C: Temperature in the mixing volume**

729 The energy conservation for evaporating droplets can be written as

730 $$(T - T_{m0})(1 + q_{vm})c_{pm} + (1-\mu)\delta q^* L = 0 \quad \text{(C1)}$$

731 here c_{pm} is the specific heat capacity of the moist air

732 $$c_{pm} = \frac{c_{pa} + q_{vm}c_{pv}}{1 + q_{vm}} \quad \text{(C2)}$$

733 Since $q_{vm} \ll 1$ and, $c_{pa} \cong c_{pm}$ Eq.(C1) may be simplified, so that the final temperature after mixing

734 $$T = T_{m0} - \frac{(1-\mu)\delta q^* L}{c_{pa}} \quad \text{(C3)}$$

735 For the case when $T_1 \neq T_2$ Eq. (C3) should be replaced by

$$T = T_{m0} - \frac{\delta q_m L}{c_{pa}} \quad \text{(C4)}$$

Eqs. (C3) and (C4) are valid for the mixing fraction $\mu > \mu_{cr}$. For $\mu \leq \mu_{cr}$ all entrained liquid water μq_0 evaporates, and the final temperature will be

$$T = T_{m0} - \frac{\mu q_0 L}{c_{pa}} \quad \text{(C5)}$$

References

Andrejczuk M., Grabowski, W. W., Malinowski, S. P., and Smolarkiewicz, P. K.: Numerical simulation of cloud–clear air interfacial mixing: homogeneous vs. inhomogeneous mixing., J. Atmos. Sci., 66, 2493-2500, 2009.

Baker, M. B. and Latham, J.: The evolution of droplet spectra and the rate of production of embryonic raindrops in small cumulus clouds, J. Atmos. Sci., 36, 1612–1615, 1979.

Baker, M. B. and Latham, J.: A diffusive model of the turbulent mixing of dry and cloudy air, Q. J. R. Met. Soc., 108, 871–898, 1982.

Baker, M. B., Corbin, R. G., and Latham, J.: The influence of entrainment on the evolution of cloud droplet spectra: I. A model of inhomogeneous mixing, Q. J. Roy. Meteor. Soc., 106, 581–598, 1980.

Beals, M.J., and Fugal, J.P., Shaw, R.A., Lu, J., Spuler, S.M., Stith, J.L.: Holographic measurements of inhomogeneous cloud mixing at the centimeter scale. Science, 350, 87-90, 2015

Bohren, C. F. and Albrecht, C. H.: Atmospheric Thermodynamics, Oxford University Press, New York, 402 pp., 1998.

Bower, K. N. and Choularton, T. W.: The effects of entrainment on the growth of droplets in continental cumulus clouds, Q. J. Roy. Meteor. Soc., 114, 1411–1434, 1988.

Broadwell, J. E., and R. E. Breidenthal: A simple model of mixing and chemical reaction in a turbulent shear layer. J. Fluid Mech., 125, 397–410, 1982

Burnet, F. and Brenguier, J. L.: Observational study of the entrainment-mixing process in warm convective clouds, J. Atmos. Sci., 64, 1995–2011, 2007.

Devenish, B. J., Bartello, P., Brenguier, J.-L., Collins, L. R., Grabowski, W. W., Ijzermans, R. H. A., Malinovski, S. P., Reeks, M.W., Vassilicos, J. C.,Wang, L- P., andWarhaft, Z.: Droplet growth in warm turbulent clouds, Q. J. Roy. Meteor. Soc., 138, 1401–1429, 2012.

764 Gerber, H., Frick, G., Jensen, J. B., and Hudson, J. G.: Entrainment, mixing, and microphysics in
765 trade-wind cumulus, J. Meteorol. Soc. Jpn., 86, 87–106, 2008.
766 Hill, T. A. and Choularton, T. W.: An airbone study of the microphysical structure of cumulus clouds,
767 Q. J. Roy. Meteor. Soc., 111, 517–544, 1985.
768 Jarecka, D., Grabowski, W. W., Morrison, H., Pawlowska, H.: Homogeneity of the Subgrid-Scale
769 Turbulent Mixing in Large-Eddy Simulation of Shallow Convection. J. Atmos. Sci. 70, 2751-
770 2767, 2013
771 Jeffery, C. A.: Inhomogeneous cloud evaporation, invariance, and Damköhler number, J.Geoph.
772 Res., 112, D24S21, doi:10.1029/2007JD008789, 2007.
773 Jensen, J. and Baker, M.: A simple model of droplet spectra evolution during turbulent mixing, J.
774 Atmos. Sci., 46, 2812–2829, 1989.
775 Korolev A. V.: The influence of supersaturation fluctuations on droplet spectra formation. Journal
776 of the Atmospheric Sciences, 52, 3620-3634, 1995.
777 Korolev, A. V. and Isaac, G. A.: Drop growth due to high supersaturation caused by isobaric mixing,
778 J. Atmos. Sci., 57, 1675–1685, 2000.
779 Korolev, A. V. and I.P. Mazin,: Supersaturation of water vapor in clouds. J. Atmos. Sci., 60, 2957-
780 2974, 2003.
781 Krueger, S., Su, C.-W., and McMurtry, P.: Modeling entrainment and finescale mixing in cumulus
782 clouds, J. Atmos. Sci., 54, 2697–2712, 1997.
783 Kumar, B., Schumacher, J., and Shaw, R. A.: Cloud microphysical effects of turbulent mixing and
784 entrainment, Theor. Comput. Fluid Dyn., 27, 361–376, 2013.
785 Lasher-Trapp, S. G., Cooper, W. A., and Blyth, A. M.: Broadening of droplet size distributions from
786 entrainment and mixing in a cumulus cloud, Q. J. Roy. Meteor. Soc., 131, 195–220, 2005.
787 Latham, J. and Reed, R. L.: Laboratory studies of the effects of mixing on the evolution of cloud
788 droplet spectra, Q. J. Roy. Meteor. Soc., 103, 297–306, 1977.
789 Lehmann, K., Siebert, H., and Shaw, R. A.: Homogeneous and inhomogeneous mixing in cumulus
790 clouds: dependence on local turbulence structure, J. Atmos. Sci., 66, 3641–3659, 2009.
791 Leon, D. C., French, J. R., Lasher-Trapp, S., Blyth, A. M., Abel, S. J., Ballard, S., Bennett, L. J.,
792 Bower, K., Brooks, B., Brown, P., Choularton, T., Clark, P., Collier, C., Crosier, J., Cui, Z.,
793 Dufton, D., Eagle, C., Flynn, M. J., Gallagher, M., Hanley, K., Huang, Y., Kitchen, M., Korolev,
794 A., Lean, H., Liu, Z., Marsham, J., Moser, D., Nicol, J., Norton, E. G., Plummer, D. Price, J.,

795 Ricketts, H., Roberts, N., Rosenberg, P. D., Taylor, J. W., Williams, P. I., and Young, G.: The
796 Convective Precipitation Experiment (COPE): investigating the origins of heavy precipitation in
797 the southwestern UK, B. Am. Meteorol. Soc., in press, 2016.
798 Lu, C., and Liu Y., Niu, S.: Examination of turbulent entrainmentimixing mechanisms using a
799 combined approach. J. Geoph. Res., 116, D20207, 2011.
800 Lu, C., Liu, Y., S. Niu, S., and Endo, S.: Scale dependence of entrainment-mixing mechanisms in
801 cumulus clouds, J. Geophys. Res. Atmos., 119, 13,877-13,890, doi:10.1002/2014JD022265, 1014
802 Paluch, I. R.: Mixing and the droplet size spectrum: generalizations from the CCOPE data, J. Atmos.
803 Sci., 43, 1984–1993, 1986.
804 Paluch, I. R. and Baumgardner, D. G.: Entrainment and fine-scale mixing in a continental convective
805 cloud, J. Atmos. Sci., 46, 261–278, 1989.
806 Paluch, I. R. and Knight, C. A.: Mixing and evolution of cloud droplet size spectra in a vigorous
807 continental cumulus, J. Atmos. Sci., 41, 1801–1815, 1984.
808 Pinsky, M., Khain, A., Korolev, A., and Magaritz-Ronen, L.: Theoretical investigation of mixing in
809 warm clouds – Part 2: Homogeneous mixing, Atmos. Chem. Phys. Discuss., 15, 30269-30320,
810 doi:10.5194/acpd-15-30269-2015, 2016.
811 Pinsky, M., Khain, A., and Korolev, A.: Theoretical analysis of mixing in liquid clouds – Part 3:
812 Inhomogeneous mixing, Atmos. Chem. Phys. Discuss., 15, 30321–30381, doi:10.5194/acpd-15-
813 30321-2015, 2016.
814 Rogers, R. R.: A Short Course in Cloud Physics, Pergamon press, Oxford, 227 pp., 1976.
815 Squires, P.: The growth of cloud drops by condensation. Aust. J. Sci. Res., 5, 66–86, 1952.
816 Su, C.-W., Krueger, S. K., McMurtry, P. A., and Austin, P. H.: Linear eddy modeling of droplet
817 spectral evolution during entrainment and mixing in cumulus clouds, Atmos. Res., 47-48, 41-58,
818 1998.
819 Tolle, M. H., and S. K. Krueger, Effects of entrainment and mixing on droplet size distributions in
820 warm cumulus clouds, J. Adv. Model. Earth Syst., 6, 281–299, doi:10.1002/ 2012MS000209,
821 2014.

822 **Table 1**

823 **List of Symbols**

Symbol	Description	Units
A_2	$\frac{pR_v}{e_s R_a} + \frac{L^2}{c_{pa} R_v T^2}$	-
a	$\frac{e_s R_a L^2}{p c_{pa} R_v^2 T^2}$	-
b	$\frac{c_{pa} R_v T^2}{L^2}$	-
c_{pa}	specific heat capacity of dry air at constant pressure	J kg^{-1}K^{-1}
c_{pv}	specific heat capacity of water vapor at constant pressure	J kg^{-1}K^{-1}
$\overline{D}$	mean droplet diameter	m
D_2	mean square droplet diameter	m
D_v	mean volume droplet diameter	m
e	water vapor pressure	N m^{-2}
e_1	initial water vapor pressure in the cloud parcel	N m^{-2}
e_2	initial water vapor pressure in the entrained sub-saturated parcel	N m^{-2}
e_s	saturation vapor pressure above flat surface of water	N m^{-2}
$f(D)$	size distribution of cloud droplets normalized on unity	m^{-1}
L	latent heat for liquid water	J kg^{-1}
M_n	n-th moment of the droplet size distribution $\frac{\int_0^\infty f(r) r^n dr}{\int_0^\infty f(r) dr}$	m^n
N	concentration of droplets	m^{-3}
N_1	concentration of droplets before mixing	m^{-3}
p	pressure of moist air	N m^{-2}
R_a	specific gas constant of moist air	J kg^{-1}K^{-1}
R_v	specific gas constant of water vapor	J kg^{-1}K^{-1}
RH	e/E_S, relative humidity over water (saturation ratio)	-

RH_1	initial relative humidity in the cloud volume (RH_1=1)	-
RH_2	relative humidity in the entrained sub-saturated parcel	-
RH_{m0}	relative humidity after instant mixing of cloudy and entrained air, but before droplets evaporation	-
q	cloud liquid water mixing ratio (mass of liquid water per 1kg of dry air)	-
q_1	cloud liquid water mixing ratio before mixing	-
q_v	water vapor mixing ratio (mass of water vapor per 1kg of dry air)	-
S	$e/e_s - 1$, supersaturation	-
S_2	supersaturation of the dry out-of-cloud air	-
S_{m0}	supersaturation after instant mixing of cloudy and entrained air, but before droplets start evaporating	-
T	temperature	K
T_1	temperature of the cloud parcel before mixing	K
T_2	temperature of the entrained sub-saturated parcel before mixing	K
T_{m0}	temperature of the parcel after vapor mixing, but before droplet evaporation	K
β	extinction coefficient	m^{-1}
β_1	extinction coefficient before mixing	m^{-1}
δq_m	mixing ratio of liquid water required to saturate 1kg of the cloud volume after instant mixing, but before droplet evaporation.	-
δq^*	mixing ratio of liquid water required to saturate 1kg of the dry out-of-cloud air	-
μ	cloud fraction of mixing air, $0 \le \mu \le 1$	-
μ_{cr}	critical cloud fraction, such that for $\mu \le \mu_{cr}$ all droplets evaporate	-
ρ_a	density of the dry air	kg m^{-3}
ρ_w	density of liquid water	kg m^{-3}
ξ	coefficient $0 \le \xi \le 1$ characterizing proximity of homogeneous mixing to inhomogeneous (when $\xi \to 0$).	-

824

Figure Captions

Figure 1. Classical conceptual diagram of (a) inhomogeneous and (b) homogeneous mixing. 1 initial state; 2 mixing state; 3 final state.

Figure 2. Dependence of critical mixing fraction μ_{cr} versus mixing ratio q_0 calculated from Eq.(7). Circles indicate modeled points. The calculations were performed for T=0C and H=3000m.

Figure 3. Dependence of ξ versus μ. Numbers are the dimensionless ratios $\delta q^*/q_1$. Critical mixing ratios μ_{cr} are indicated by stars. Grey color indicates the area where the moments of homogeneous and extreme inhomogeneous mixing may not be segregated from in-situ measurements. Dashed line was calculated for the cloud in Figs.13-14.

Figure 4. Simulation of (a) liquid water mixing ratio, (b) droplet number concentration, (c) integral droplet diameter, (d) extinction coefficient, (e) mean volume diameter, (f) time of phase relaxation, (g) relative humidity in the mixed volume before droplet evaporation RH_{m0} and at the equilibrium state RH_m, (h) final temperature T_{m0} versus ratio of mixing μ formed after homogeneous and extreme inhomogeneous mixing between dry and cloudy parcel with monodisperse droplets. Black stars indicate critical mixing fraction μ_{cr} calculated from Eq.(7). The calculations were performed for RH_2 = 0.2, 0.5, 0.8, 0.95; D_1=20μm, N_1=500cm^{-3}; $T_1 = T_2$ =0C; H=1000m.

Figure 5. Dependence of normalized liquid water mixing ratio q/q_1 (a,d,g), extinction coefficient β/β_1 (b,e,h) and mean volume diameter D_v/D_{v1} (c,f,j) versus normalized number concentration N/N_1 for various humidity of the entrained air (a,b,c), for various liquid water mixing ratios (d,e,f) and for various temperatures (g,h,j). The calculations were performed the initial conditions: H=1000m, D_1=20μm; for (a-c) $T_1 = T_2 = 0$C, N_1=500cm^{-3}; (d-f) $T_1 = T_2 = 0$C, RH_2 =0.5; (g-j) $T_1 = T_2 = T$, N_1=500cm^{-3}, RH_2 =0.5.

Figure 6. Simulation of (a) droplet number concentration and (b) liquid water mixing ratio, (c) integral droplet diameter, (d) extinction coefficient, (e) mean volume diameter, (f) time of phase relaxation, (g) relative humidity in the mixed volume before droplet evaporation RH_{m0} and at the equilibrium state RH_m, (h) final temperature T_m versus ratio of mixing μ formed after homogeneous and extreme inhomogeneous mixing between dry and cloudy parcel with monodisperse droplets. The calculations were performed for RH_2=0.9; D_1=10μm, N_1=500cm^{-3}; T_1 =0C; T_2 = -10C, -5C, 0C; H=1000m.

Figure 7. Effect of temperature difference between cloud and entrained air on mixing. The calculations were performed for initial temperatures T_2: (1) -10C; (2) -5C; (3) 0C. Grey circles indicate extreme inhomogeneous mixing on line 1 at the AB interval. The rest cases on extreme inhomogeneous mixing are indicated by open circles. The initial conditions used for the calculations were: H=1000m, RH_2=90%; D_1 =10μm, N_1 =500cm^{-3}, T_1=0C.

Figure 8. Conceptual diagram of cascade mixing of the out-of-cloud entrained parcel with the cloudy environment

Figure 9. Simulation of stochastic mixing corresponding to stages 1-4 as indicated in Fig.8. Solid red lines indicate the normalized dependences q, β, D_v vs. N for the primary stage of homogeneous mixing. Dashed red lines indicate the same dependences for inhomogeneous mixing. The initial conditions used for the simulations were: H=1000m, $T_1 = T_2$ =0C; RH_2=0.5; D_1 =10μm, N_1 =500cm^{-3}.

Figure 10. Conceptual diagram explaining breaking the functional relationships between the microphysical moment during progressive missing (see text).

Figure 11. Droplet size distributions formed during the progressive homogeneous mixing corresponding to the (a,e) primary stage; (b,f) 2nd stage; (c,g) 3rd stage; (d,h) 4th stage. Left column (a,b,c,d) corresponds to the case, when the cloud temperature is equal to the dry air temperature $T_1 = T_2 = 0$℃,; right column (e,f,g,h) corresponds to the case when $T_1 = 0$℃, $T_2 = -10$℃. For both cases the simulation was performed for D_1 =10μm; N=500cm^{-3}; RH_2=0.9.

Figure 12. Conceptual diagrams of scattering of measurements of q versus N for (a) extreme inhomogeneous and (b) homogeneous mixing.

Figure 13. Spatial changes of particle concentration (a), extinction coefficeint (b), liquid water content (c) and average and mean mass diameter (d) during transit through one of the convective clouds measured by CDP. The measurements were conducted during the COPE-MED project on 18 July, 2015. The sampling rate 10Hz (~10m spatial resolution). H=5500m, T=-12C, RH=0.2.

Figure 14. Relatonships between (a) $LWC(N)$; (b) $\beta(N)$; (c) $D_v(N)$; (d) $LWC(\beta)$ calculated from the CDP measurements obtained during sampling several convective clouds. The meadurements were conducted during the COPE-MED project on 18 July, 2015, H=5500m, T=-12C, RH=0.2. The measurements were sampled at 10Hz (~10m spatial resolution).

Dashed lines are linear regressions. Red lines indicate primary inhomogeneous mixing dependencies calculated for the same environmental conditions.

Figure 15. Relatonships between (a) $LWC(N)$; (b) $\beta(N)$; (c) $D_v(N)$; (d) $LWC(\beta)$ calculated from the CDP measurements sampled during traverse through 45 convective clouds. The meadurements were conducted during the COPE-MED project on 02 August, 2015. Dashed lines indicate (a), (b) and (d) indicate the sectors, where the majority of the points are scattered. The altitude of sampling varied in the range 3000m <H< 4500m, temperature -11C<T<0C, relative humidity in the vicinity of clouds 15%<RH<65%. The measurements were sampled at 10Hz (~10m spatial resolution).

Figure A1. Amount of evaporated liquid water δq_m required for saturation of a cloud volume with initial humidity RH_{m}. Comparisons of the modeled δq_m and that calculated from Eqs. (A8) and (A9) for three temperatures T_{m0} =-20C, 0C and 20C. Calculations were performed for P=880mb.

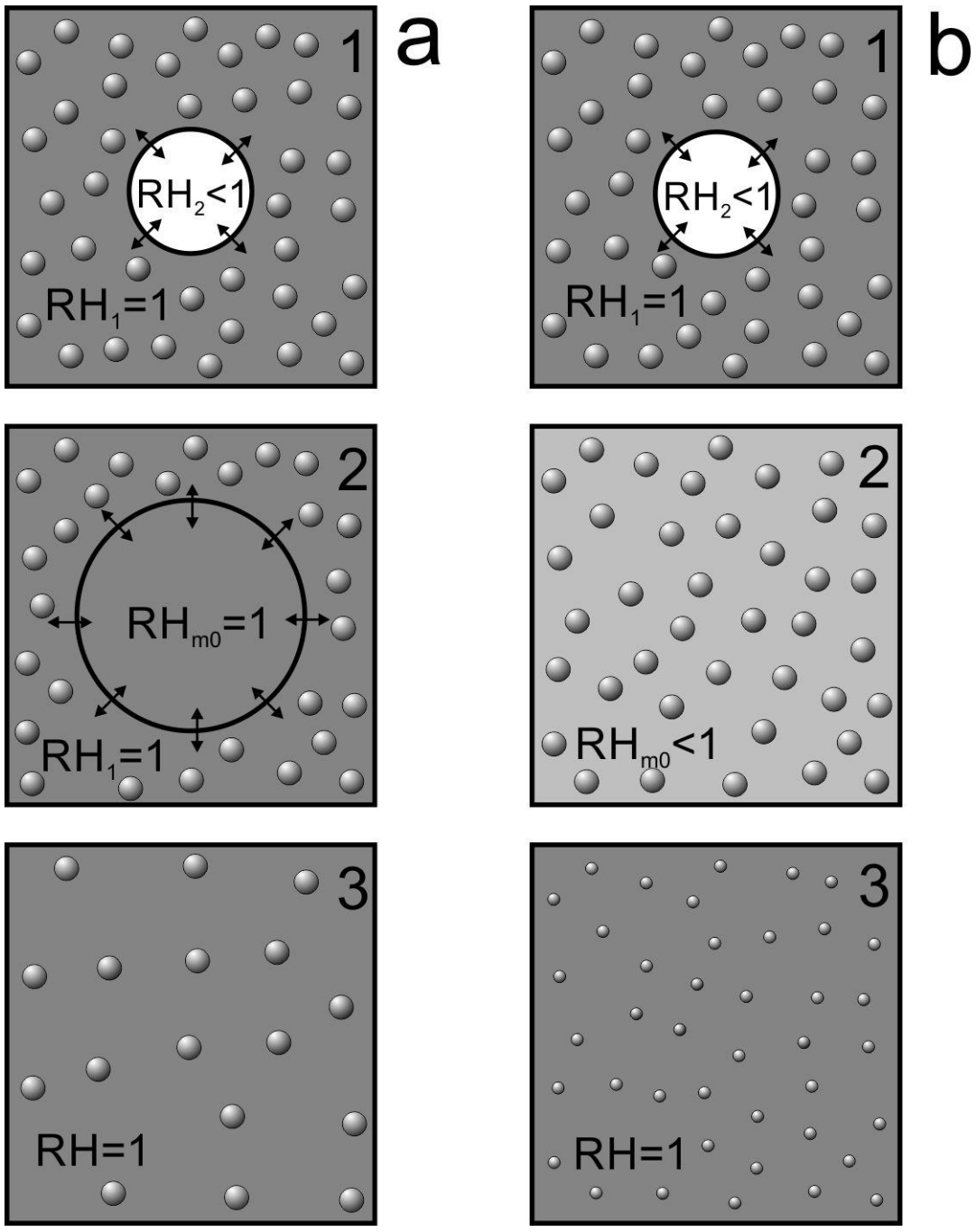

Figure 1. Classical conceptual diagram of (a) inhomogeneous and (b) homogeneous mixing. 1 initial state; 2 mixing state; 3 final state.

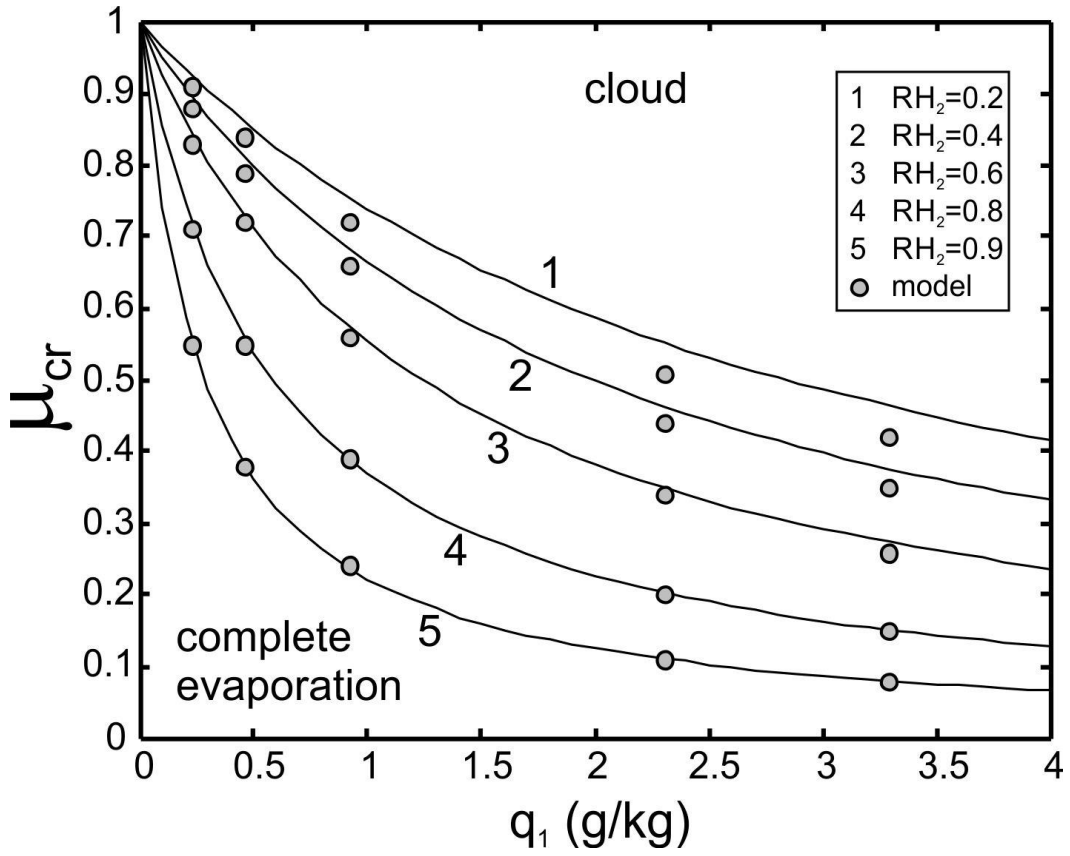

Figure 2. Dependence of critical mixing fraction μ_{cr} versus mixing ratio q_0 calculated from Eq.(7). Circles indicate modeled points. The calculations were performed for T=0C and H=3000m.

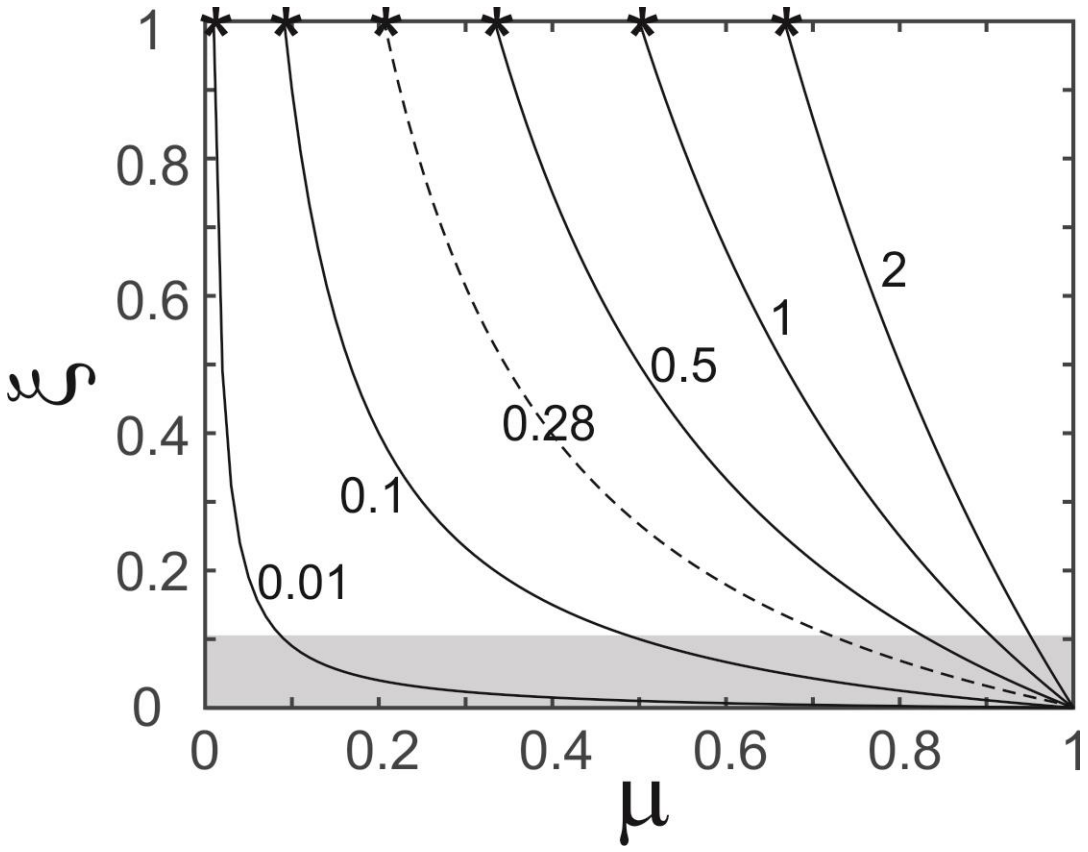

Figure 3. Dependence of ξ versus μ. Numbers are the dimensionless ratios $\delta q^*/q_1$. Critical mixing ratios μ_{cr} are indicated by stars. Grey color indicates the area where the moments of homogeneous and extreme inhomogeneous mixing may not be segregated from in-situ measurements. Dashed line was calculated for the cloud in Figs.13-14.

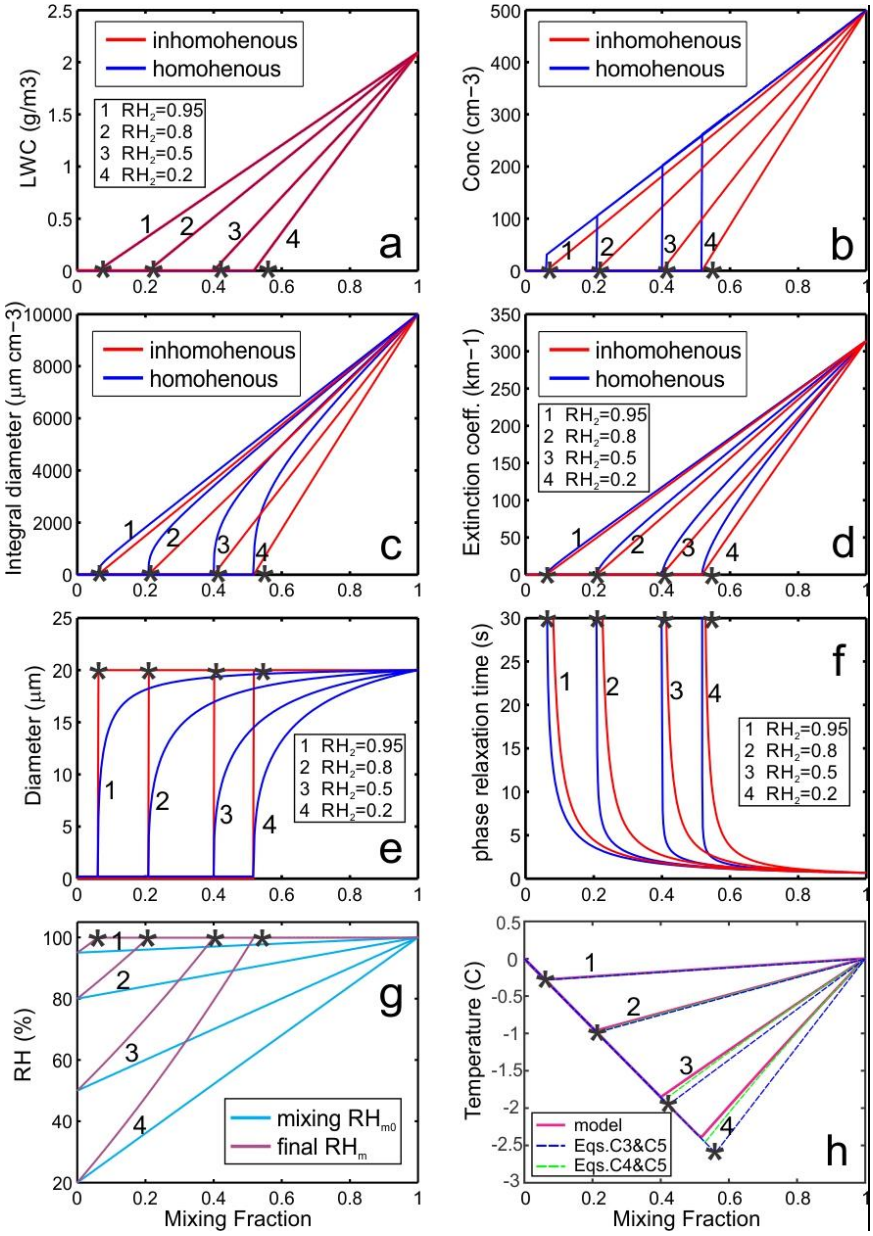

Figure 4. Simulation of (a) liquid water mixing ratio, (b) droplet number concentration, (c) integral droplet diameter, (d) extinction coefficient, (e) mean volume diameter, (f) time of phase relaxation, (g) relative humidity in the mixed volume before droplet evaporation RH_{m0} and at the equilibrium state RH_m, (h) final temperature T_{m0} versus ratio of mixing μ formed after homogeneous and extreme inhomogeneous mixing between dry and cloudy parcel with monodisperse droplets. Black stars indicate critical mixing fraction μ_{cr} calculated from Eq.(7). The calculations were performed for RH_2 =0.2, 0.5, 0.8, 0.95; D_1=20μm, N_1=500cm^{-3}; $T_1 = T_2$ =0C; H=1000m.

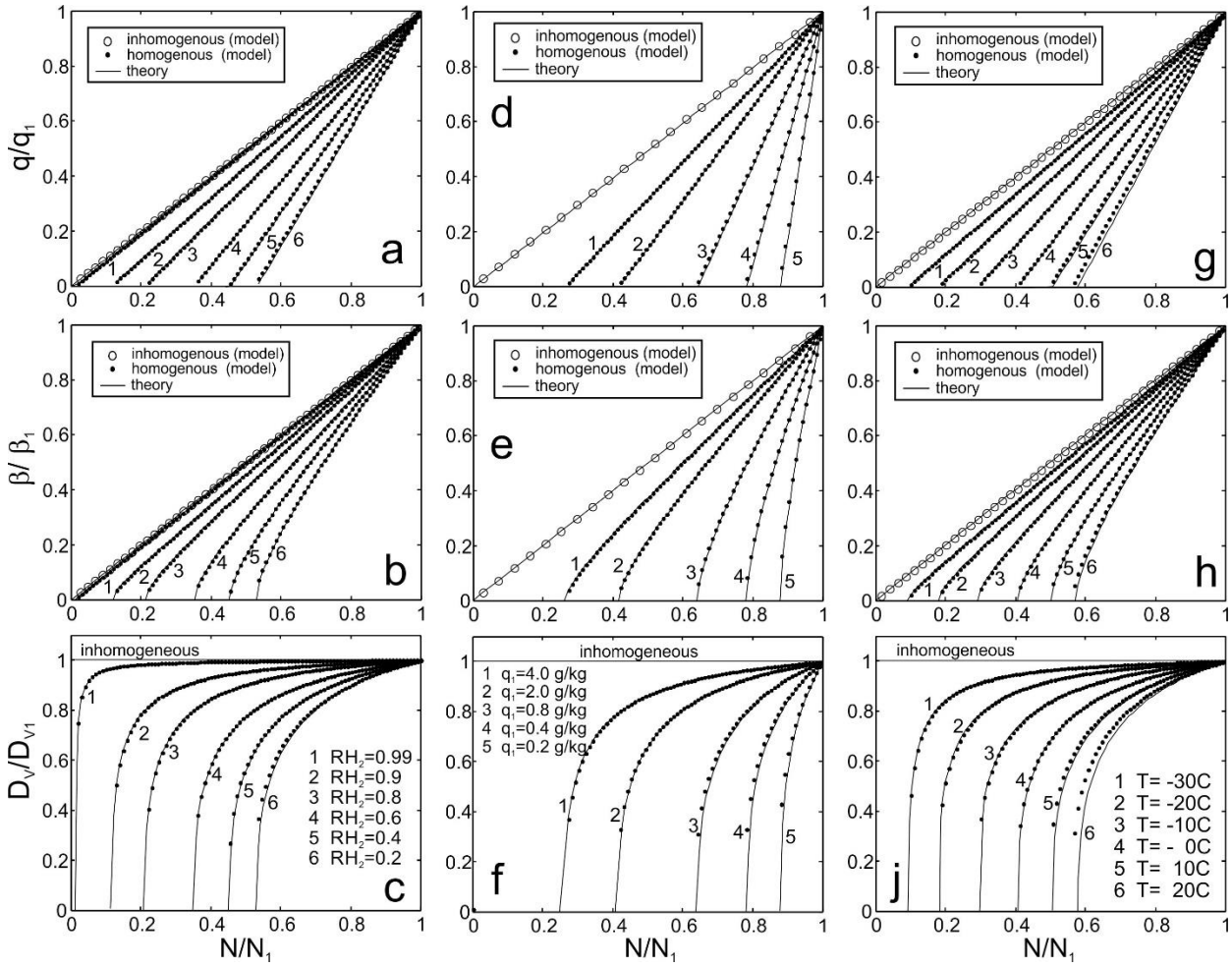

Figure 5. Dependence of normalized liquid water mixing ratio q/q_1 (a,d,g), extinction coefficient β/β_1 (b,e,h) and mean volume diameter D_v/D_{v1} (c,f,j) versus normalized number concentration N/N_1 for various humidity of the entrained air (a,b,c), for various liquid water mixing ratios (d,e,f) and for various temperatures (g,h,j). The calculations were performed the initial conditions: H=1000m, D_1=20μm; for (a-c) $T_1 = T_2 = 0$C, N_1=500cm^{-3}; (d-f) $T_1 = T_2 = 0$C, RH_2 =0.5; (g-j) $T_1 = T_2 = T$, N_1=500cm^{-3}, RH_2 =0.5.

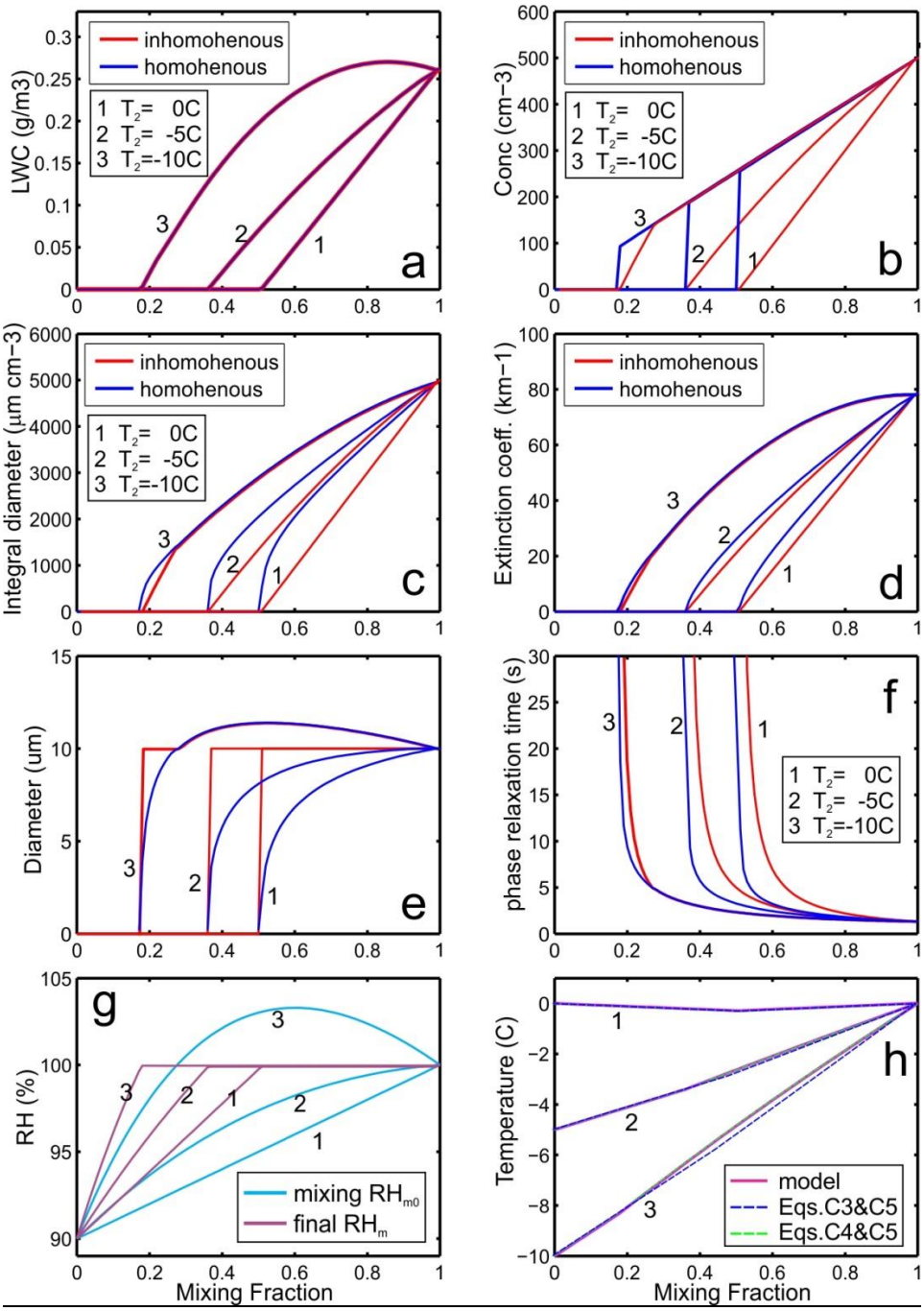

Figure 6. Simulation of (a) droplet number concentration and (b) liquid water mixing ratio, (c) integral droplet diameter, (d) extinction coefficient, (e) mean volume diameter, (f) time of phase relaxation, (g) relative humidity in the mixed volume before droplet evaporation RH_{m0} and at the equilibrium state RH_m, (h) final temperature T_m versus ratio of mixing μ formed after homogeneous and extreme inhomogeneous mixing between dry and cloudy parcel with monodisperse droplets. The calculations were performed for RH_2=0.9; D_1=10μm, N_1=500cm^{-3}; T_1 =0C; T_2 = -10C, -5C, 0C; H=1000m.

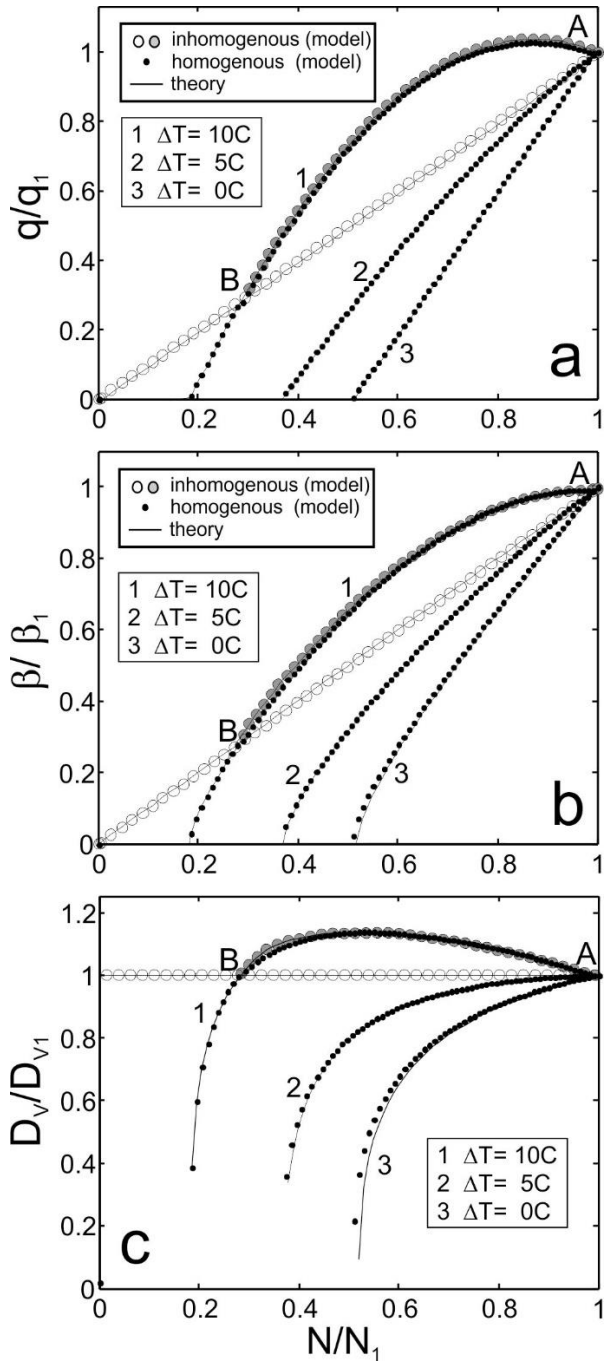

Figure 7. Effect of temperature difference between cloud and entrained air on mixing. The calculations were performed for initial temperatures T_2: (1) -10C; (2) -5C; (3) 0C. Grey circles indicate extreme inhomogeneous mixing on line 1 at the AB interval. The rest cases on extreme inhomogeneous mixing are indicated by open circles. The initial conditions used for the calculations were: H=1000m, RH_2=90%; D_1 =10μm, N_1 =500cm^{-3}, T_1=0C.

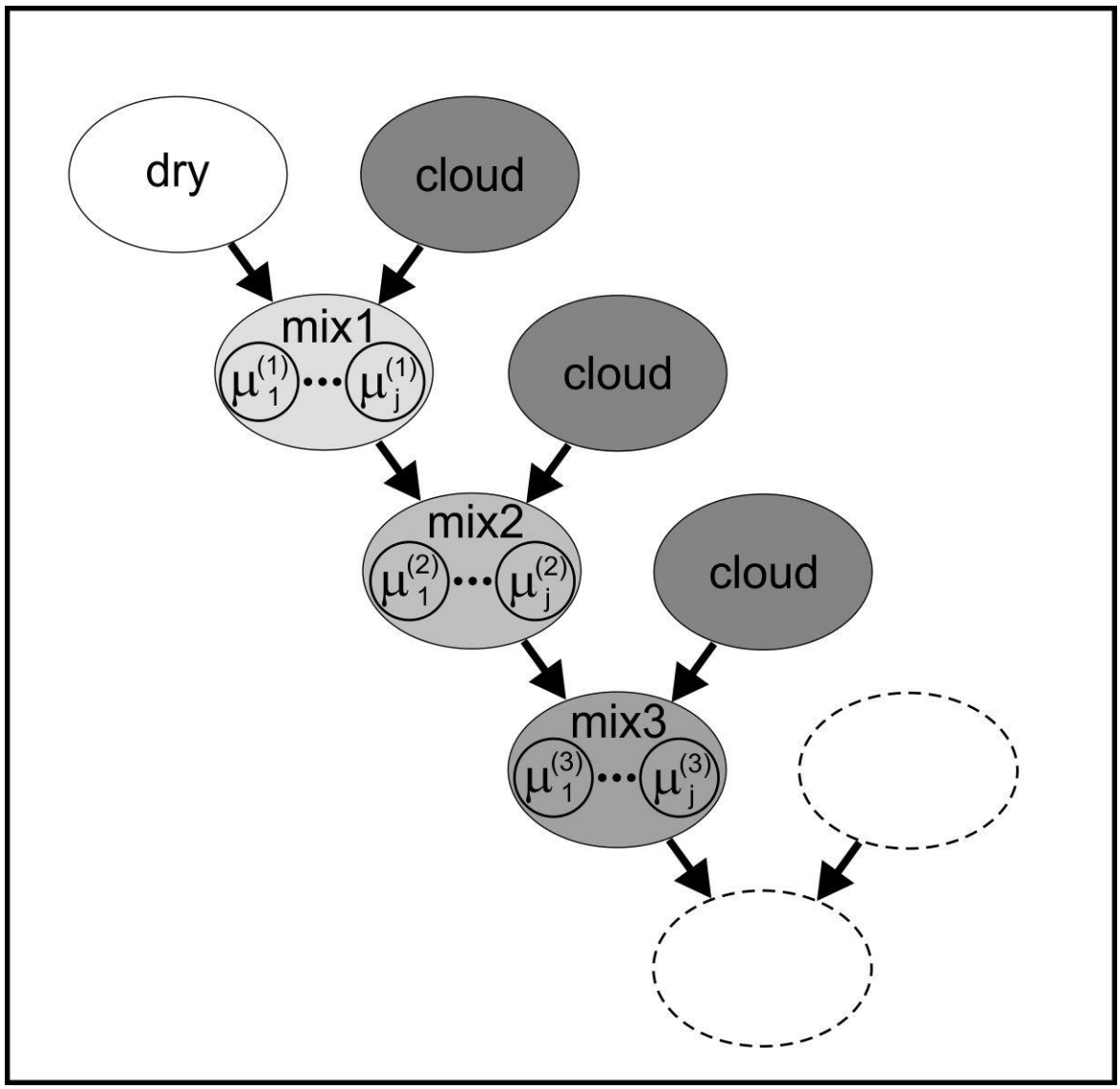

Figure 8. Conceptual diagram of cascade mixing of the out-of-cloud entrained parcel with the cloudy environment.

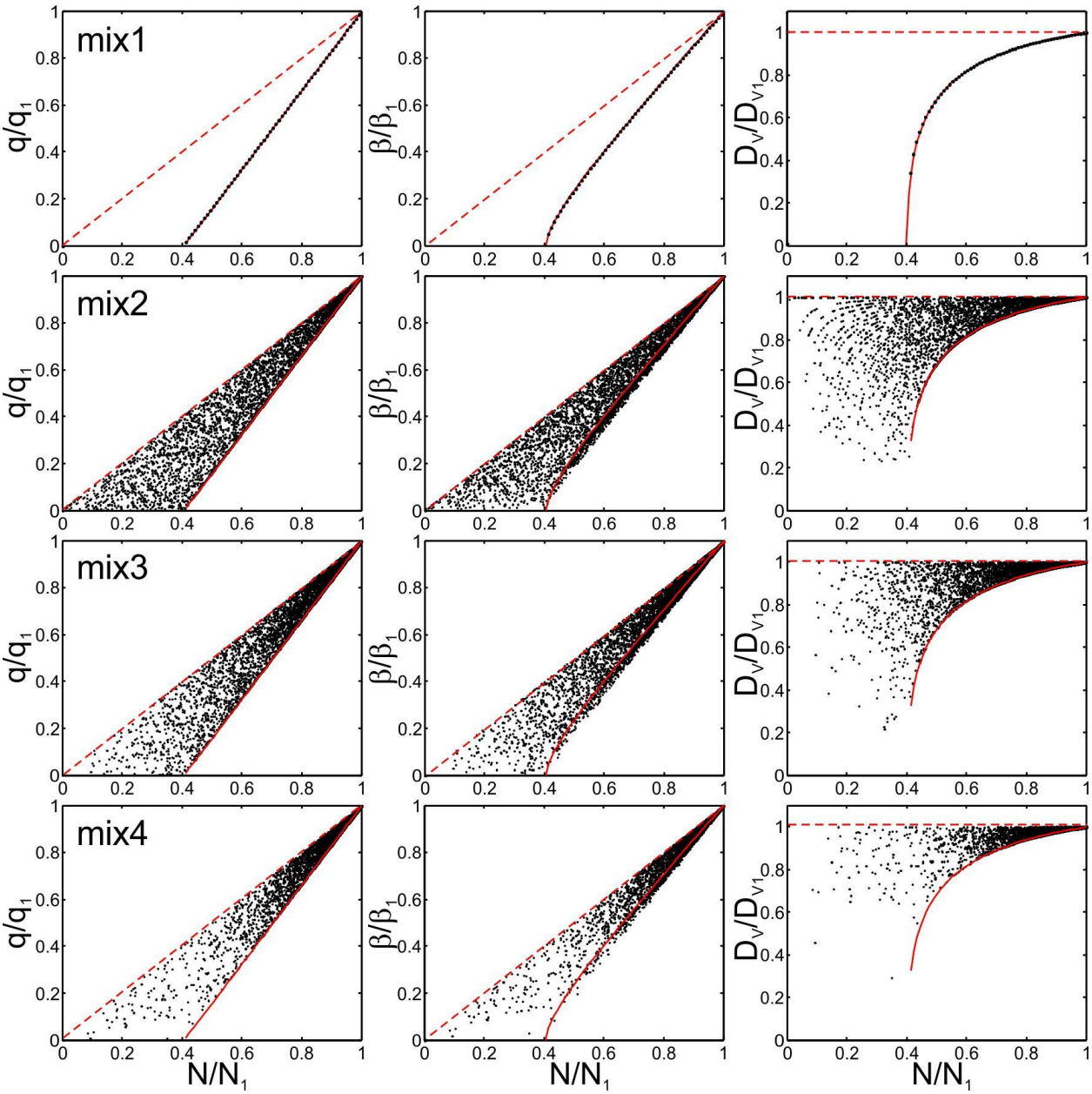

Figure 9. Simulation of stochastic mixing corresponding to stages 1-4 as indicated in Fig.8. Solid red lines indicate the normalized dependences q, β, D_v vs. N for the primary stage of homogeneous mixing. Dashed red lines indicate the same dependences for inhomogeneous mixing. The initial conditions used for the simulations were: H=1000m, $T_1 = T_2$ =0C; RH_2=0.5; D_1 =10μm, N_1 =500cm^{-3}.

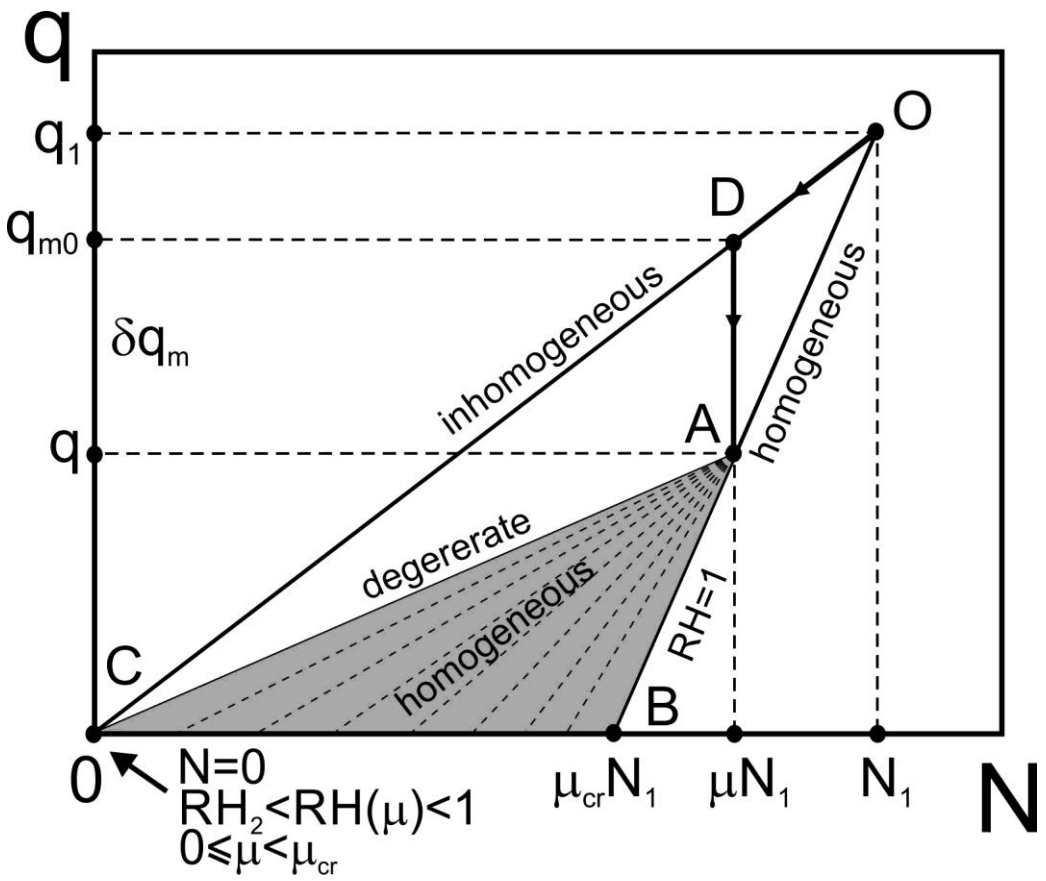

Figure 10. Conceptual diagram explaining breaking the functional relationships between the microphysical moment during progressive missing (see text).

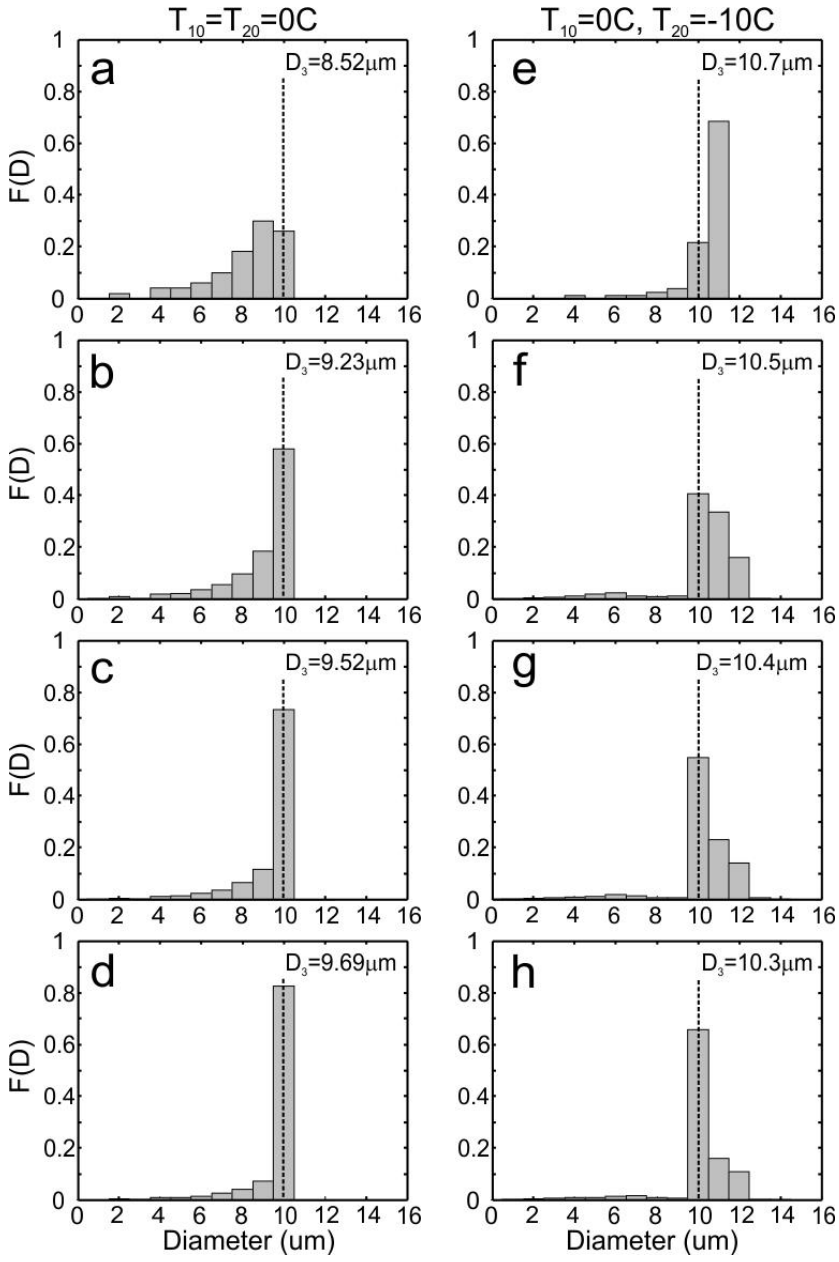

Figure 11. Droplet size distributions formed during the progressive homogeneous mixing corresponding to the (a,e) primary stage; (b,f) 2nd stage; (c,g) 3rd stage; (d,h) 4th stage. Left column (a,b,c,d) corresponds to the case, when the cloud temperature is equal to the dry air temperature $T_1 = T_2 = 0$°C,; right column (e,f,g,h) corresponds to the case when $T_1 = 0$°C, $T_2 = -10$°C. For both cases the simulation was performed for D_1 =10μm; N=500cm^{-3}; RH_2=0.9.

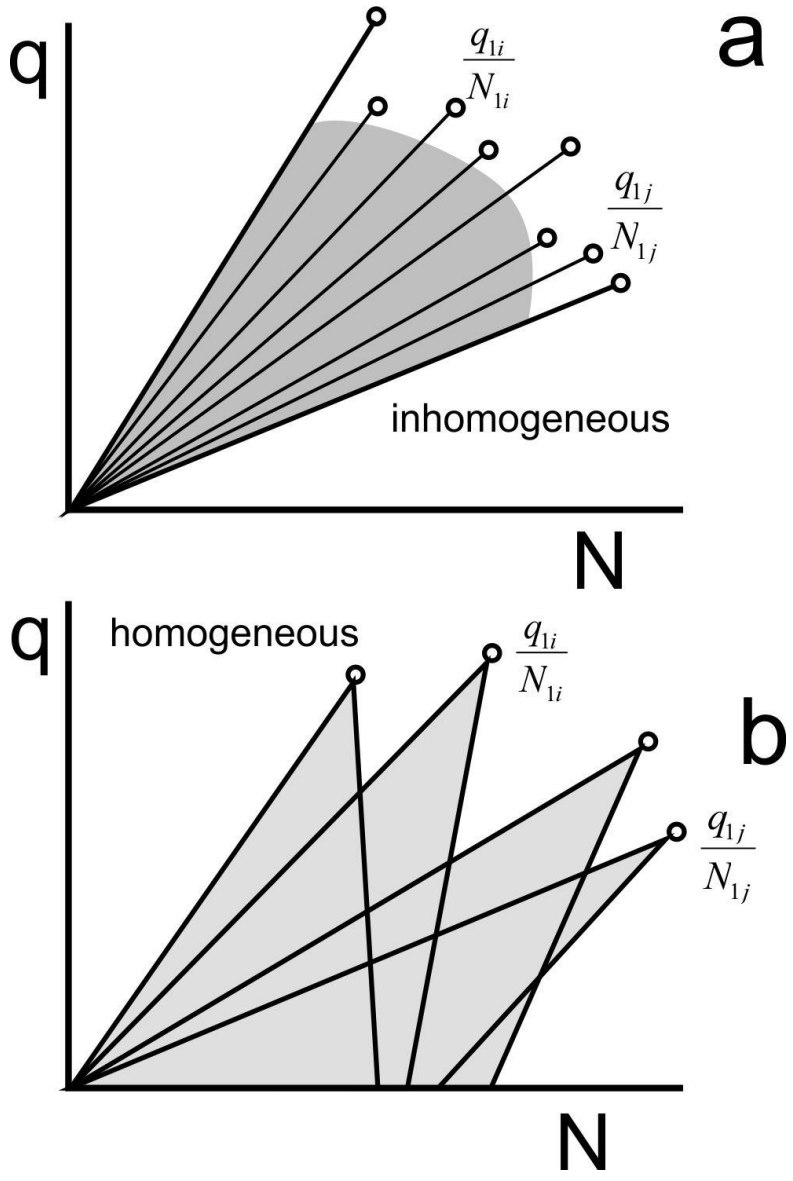

Figure 12. Conceptual diagrams of scattering of measurements of q versus N for (a) extreme inhomogeneous and (b) homogeneous mixing.

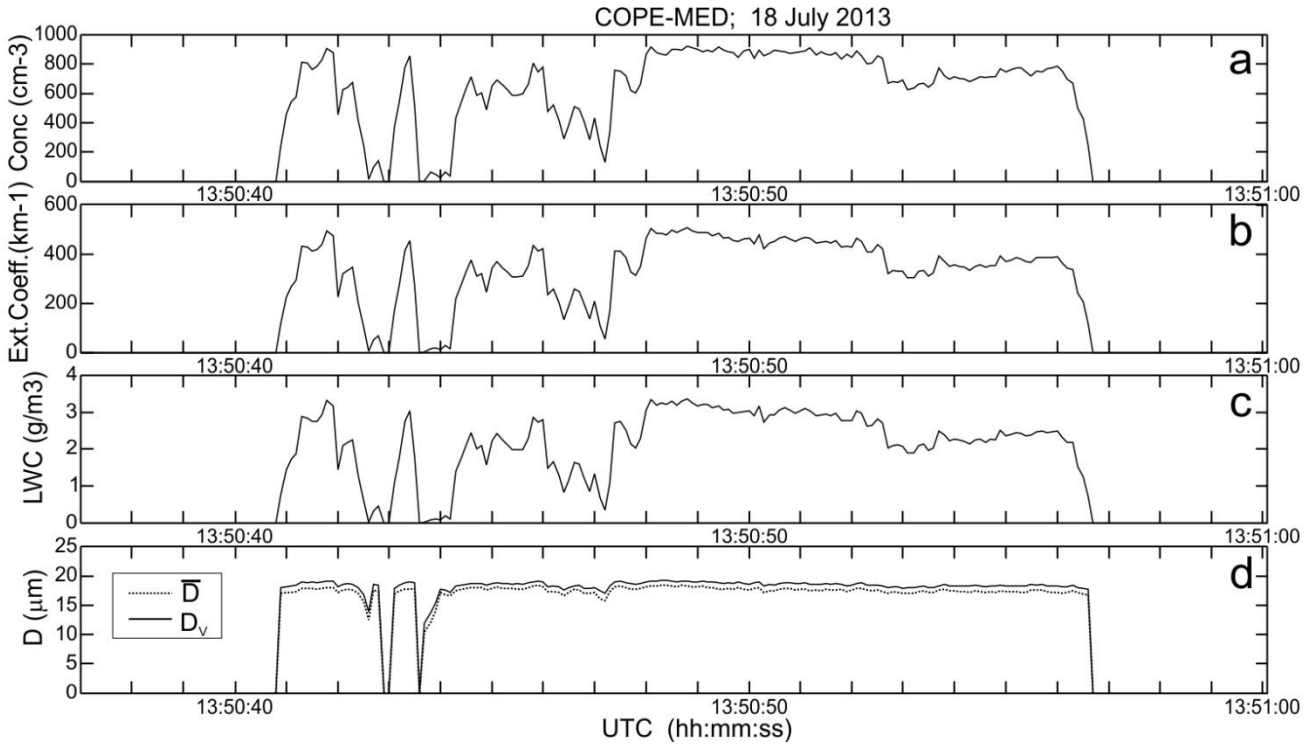

Figure 13. Spatial changes of particle concentration (a), extinction coefficeint (b), liquid water content (c) and average and mean mass diameter (d) during transit through one of the convective clouds measured by CDP. The measurements were conducted during the COPE-MED project on 18 July, 2015. The sampling rate 10Hz (~10m spatial resolution). H=5500m, T=-12C, RH=0.2.

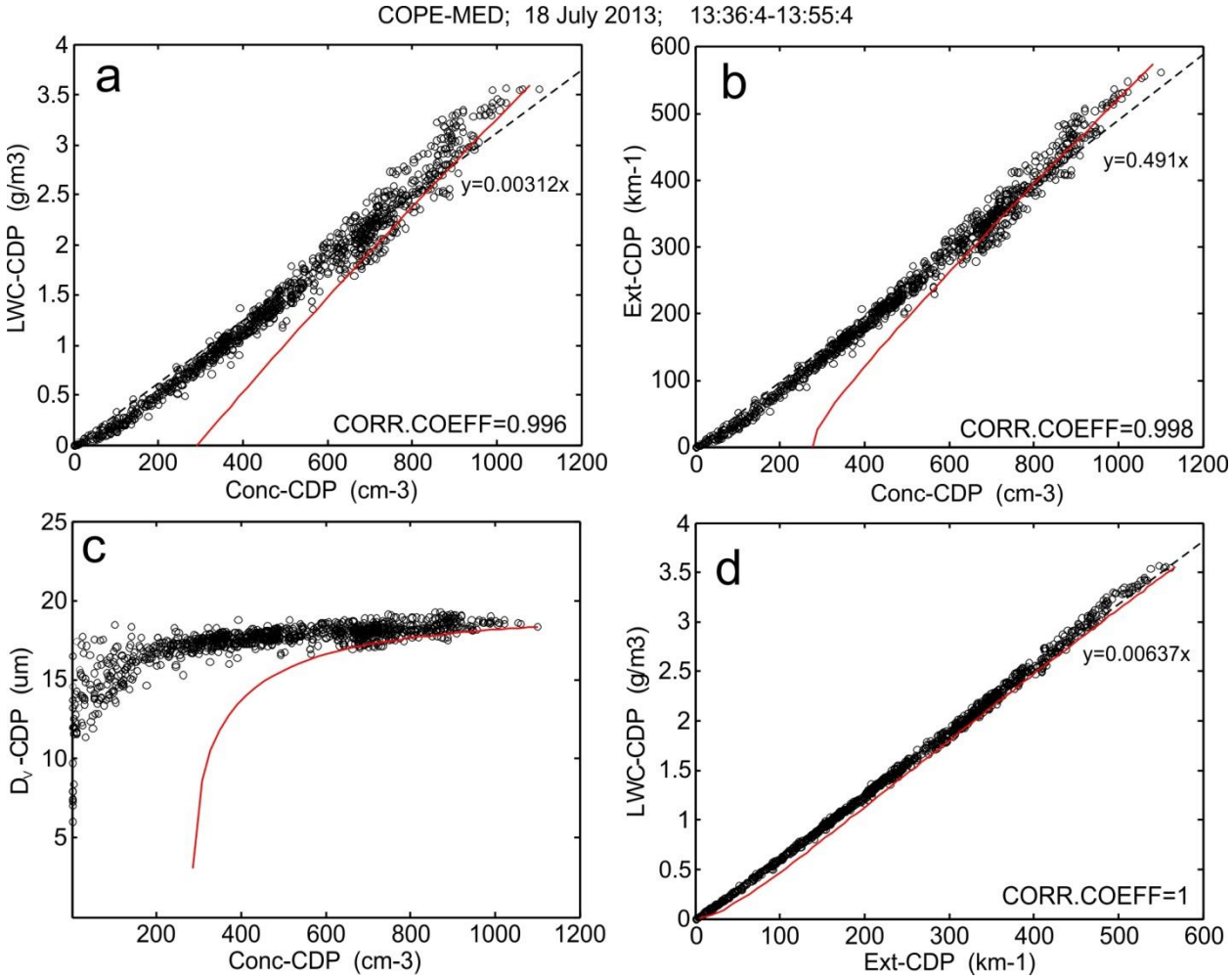

Figure 14. Relatonships between (a) $LWC(N)$; (b) $\beta(N)$; (c) $D_v(N)$; (d) $LWC(\beta)$ calculated from the CDP measurements obtained during sampling several convective clouds. The meadurements were conducted during the COPE-MED project on 18 July, 2015, H=5500m, T=-12C, RH=0.2. The measurements were sampled at 10Hz (~10m spatial resolution). Dashed lines are linear regressions. Red lines indicate primary inhomogeneous mixing dependencies calculated for the same environmental conditions.

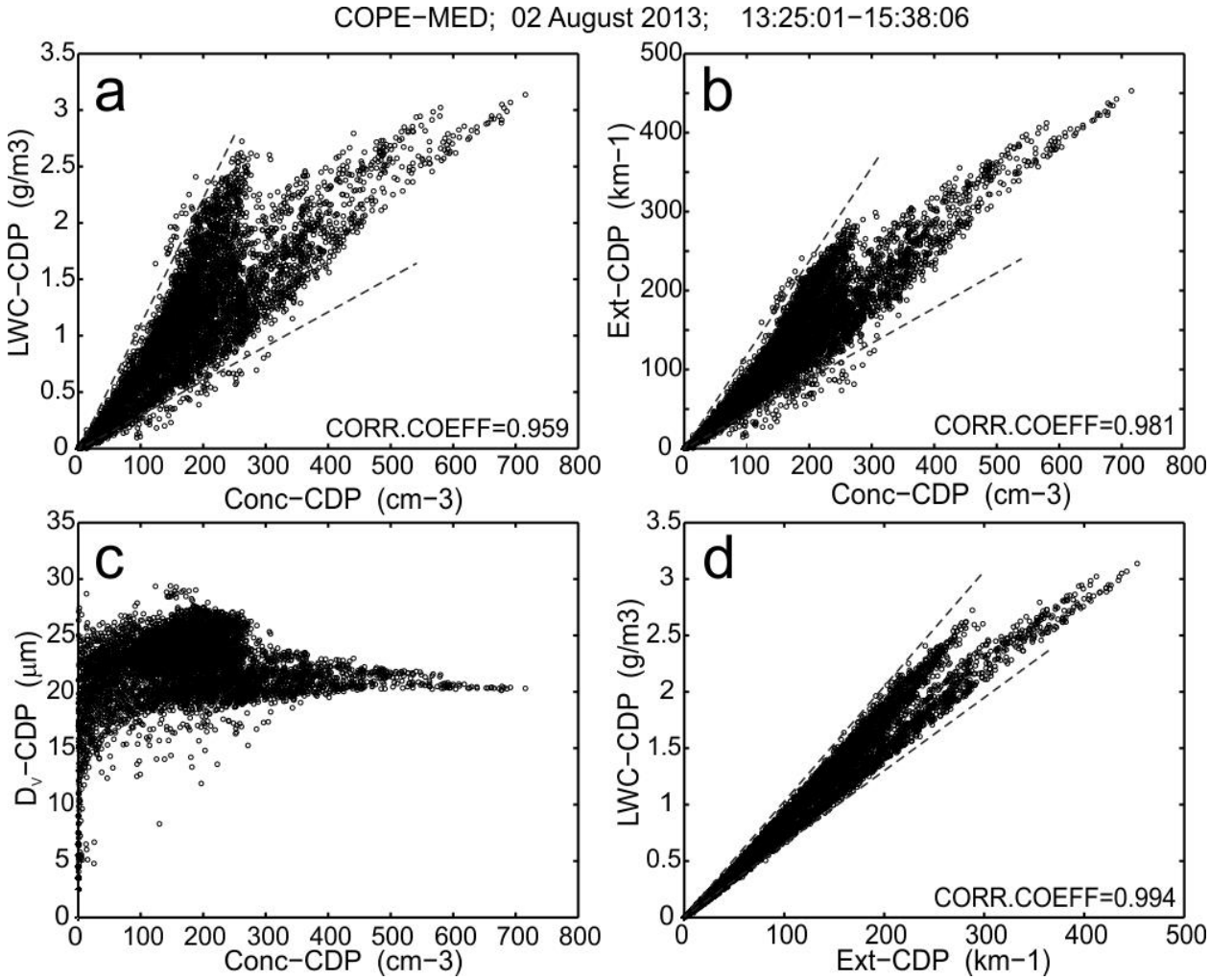

Figure 15. Relatonships between (a) $LWC(N)$; (b) $\beta(N)$; (c) $D_v(N)$; (d) $LWC(\beta)$ calculated from the CDP measurements sampled during traverse through 45 convective clouds. The meadurements were conducted during the COPE-MED project on 02 August, 2015. Dashed lines indicate (a), (b) and (d) indicate the sectors, where the majority of the points are scattered. The altitude of sampling varied in the range 3000m <H< 4500m, temperature -11C<T<0C, relative humidity in the vicinity of clouds 15%<RH<65%. The measurements were sampled at 10Hz (~10m spatial resolution).

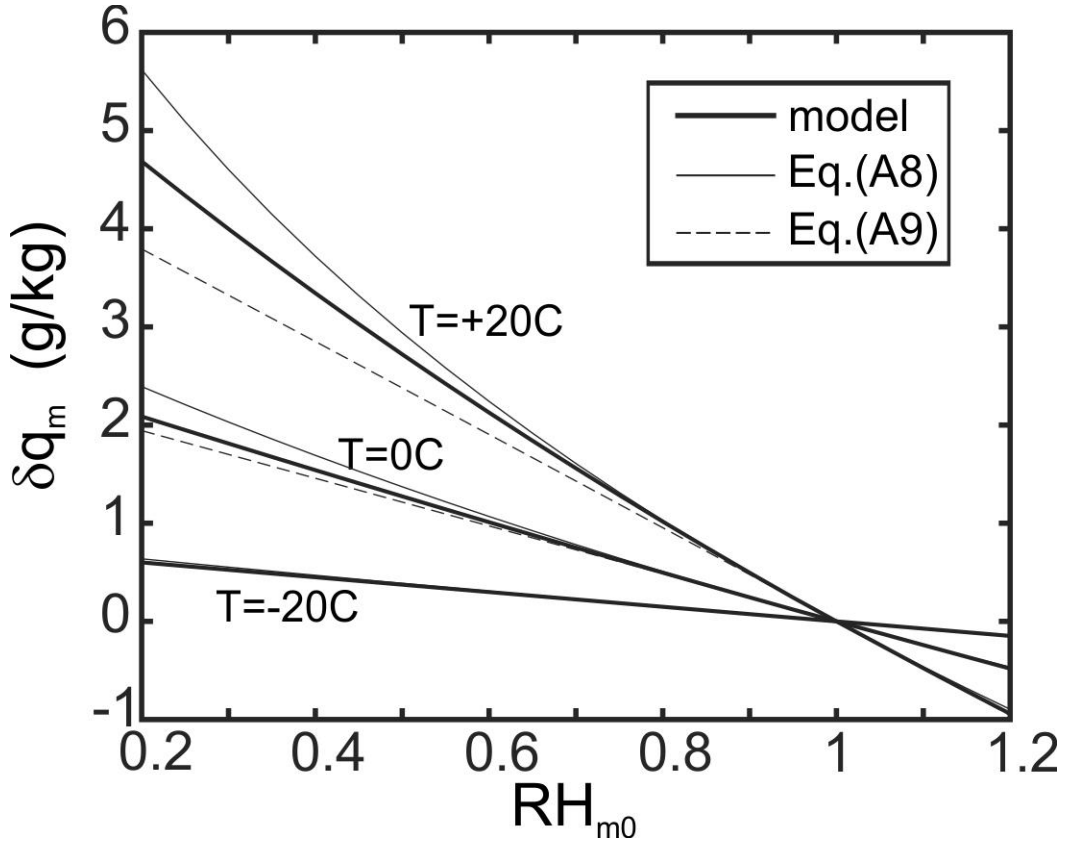

Figure A1. Amount of evaporated liquid water δq_m required for saturation of a cloud volume with initial humidity RH_{m}. Comparisons of the modeled δq_m and that calculated from Eqs. (A8) and (A9) for three temperatures T_{m0} =-20C, 0C and 20C. Calculations were performed for P=880mb.